ChemPubSoc Europe

DOI: 10.1002/slct.201700677

Chemistry SELECT Full Papers

Medicinal Chemistry & Drug Discovery

Pyridopyrimidinone Derivatives as DNAG-Quadruplex-Stabilizing Agents: Design, Synthesis and Biophysical Studies

Rajesh Malhotra[+],[a] Chhanda Rarhi[+],[b] K. V. Diveshkumar[+],[c] P. Bommisetti,[c] Sushree Prangya P. Pany,[c] Subho Roy,[b] P. I. Pradeepkumar,*[c] and Mrinalkanti Kundu*[b]

DNA can fold into non-canonical structures such as G-quadruplexes (G4 s) in addition to adopting the double helical structure. Considering the relationship between stabilization of G4 structure and anticancer effects, development of G4 interactive compounds has been of significant interest. Past years have witnessed the discovery of scaffolds targeting G4 structures based on planar, multi-aromatic ring compounds. With an aim to engineer drug-like properties, we designed and synthesized pyridopyrimidinone based selective G4 DNA stabilizing agents **1–3**, and further they were evaluated for G4 DNA recognition properties. CD melting studies revealed the preferential stabilization of parallel topology of promoter *c-MYC* and *c-KIT* G4 DNAs by the ligands, especially **2** and **3**, over the different topologies of telomeric G4 DNA. UV melting experiments suggested that no significant stabilization was observed for duplex DNA. Further, the results from ITC experiments substantiated the preferential stabilization of parallel topology of *c-MYC* G4 DNA over telomeric and duplex DNA by the ligands **2.** These data showed that ligand **2** has moderate binding affinity to the *c-MYC* G4 DNA and is ~49-fold and ~25-fold selective over the telomeric G4 DNA and the duplex DNA respectively. The molecular modeling and dynamics studies of the ligand **2** in complex with c-*MYC* and *c-KIT1* G4 DNAs showed that this ligand stacks on the 5′-quartet of *c-MYC* and 3′-quartet of *c-KIT1* G4 DNA structures.

Introduction

Anticancer agents targeting DNAs are some of the most effective agents in clinical use, and have produced significant increases in the survival of cancer patients. But, unfortunately, those anticancer agents are found to be extremely toxic due to their non-specificity.[1] Consequently, much effort has been devoted in finding agents that are more selective and thus presumably will have lesser side effects. Therefore, there is considerable excitement that the identification of cancer-specific DNA targets will yield a new generation of less toxic therapeutics. Targeting non-canonical DNA secondary structures such as G4 structures is now considered as an attractive approach in drug discovery for anticancer therapy. G4 s have been implicated in biologically important roles such as genomic instability, telomerase inhibition and the regulation of gene expression.[2]

G4 structures are formed by the stacking of two or more planar G-quartets and the G-quartets are formed through the H-bond association of adjacent guanine bases by utilizing both Hoogsteen and Watson-Crick faces.[3–5] Stabilization of these G4 structures by small molecule ligands offer new opportunities in the anticancer drug development.[2,3] Typical G4-ligand features include large aromatic surfaces for end-on π-π stacking with the external surface of the G-quartet, and structural features that prevents intercalation into double-stranded (ds) DNA. Along with this, recognition was also provided by the electrostatic as well as H-bonding interactions of the neutral/cationic side chains with the loops, grooves and phosphate backbone of the G4 structure.[6]

A broad range of ligands have been reported to selectively stabilize the G4 DNA structures over the duplex DNAs,[7] but only a handful of molecules could achieve specificity toward a particular G4 topology. Along these lines, we have demonstrated that indenopyrimidine derivatives,[8] bisbenzimidazole carboxamide derivatives,[9] benzothiazole hydrazones,[10] and indolylmethyleneindanone derivatives[11] show specific stabilization of the parallel topology of *c-MYC* and *c-KIT* promoter over telomeric G4 and duplex DNAs. In continuation with our efforts to develop topology specific G4 DNA stabilizing ligands having simple structural motifs, herein we report structurally unique small drug-like molecules as potential G4 DNA stabilizing agents having pyridopyrimidinone ring coupled with benza-

[a] *Prof. R. Malhotra*[+]
Department of Chemistry
Guru Jambheshwar University of Science and Technology
Hisar, Haryana 125001, India
[b] *C. Rarhi,*[+] *Dr. S. Roy, Dr. M. Kundu*
Department of Chemistry
TCG Lifesciences Pvt. Ltd.
BN-7, Salt Lake, Sector V, Kolkata 700091, India
E-mail: mrinal.kundu@tcgls.com
[c] *Dr. K. V. Diveshkumar,*[+] *P. Bommisetti, S. P. P. Pany, Prof. P. I. Pradeepkumar*
Department of Chemistry
Indian Institute of Technology Bombay
Mumbai 400076, India
E-mail: pradeep@chem.iitb.ac.in
[+] *The authors contributed equally*

Supporting information for this article is available on the WWW under https://doi.org/10.1002/slct.201700677

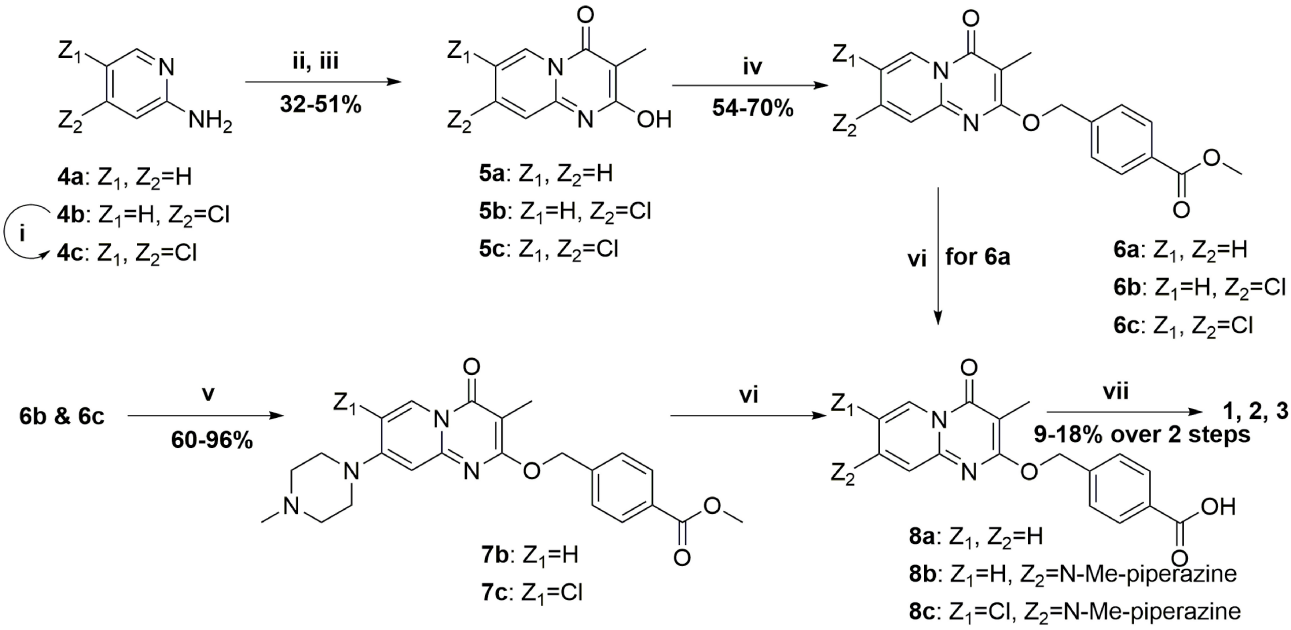

Scheme 1. Synthesis of ligands **1**, **2** and **3.** Reagents and conditions: (i) **4b**, NCS, ethyl acetate, RT, 24 h; (ii) diethyl methyl malonate, 140 °C, 24 h; (iii) diphenyl ether, 160 °C, 24 h; (iv) K_2CO_3, 4-bromomethyl-benzoic acid methyl ester, acetone, 65 °C, 3 h; (v) dipotassium hydrogenphosphate, *N*-methylpiperazine, DMSO, 110 °C, 1.5 h; (vi) LiOH, THF-MeOH-H_2O (3:2:1, v/v), RT, 3 h; (vii) EDCI.HCl - HOBT, DIPEA, *N*′,*N*′-dimethylethane-1,2-diamine, DMF, RT, 5 h.

mide units as common core structure. The binding interaction, stability and selectivity of the synthesized ligands toward G4 (*c-MYC*, *c-KIT* and telomeric) and duplex DNAs have been explored by various biophysical studies such as CD titration, CD melting, Isothermal titration calorimetry (ITC) and molecular modeling and dynamics.

Results and Discussion

Synthesis

The three ligands were synthesized following the synthetic route depicted in Scheme 1 starting from commercially available **4a** and **4b.** Compound **4c** was synthesized from **4b** using *N*-chloro succinamide (NCS) in 90% yield. Second step was performed in diethyl methyl malonate at 140 °C over a period of 24 h and the crude intermediates were then subjected to thermal cyclization (160 °C) to yield the corresponding 2-hydroxy-3-methyl-pyrido[1,2-a]pyrimidin-4-one derivatives **5a,**[12] **5b** and **5c** in varying yields over two steps. *O*-benzylation of these derivatives was done using 4-bromomethyl-benzoic acid methyl ester to obtain **6a–c** in 54–70% yields. For the ligands **2** and **3**, *N*-methylpiperazine moiety was introduced on the intermediates **6b** and **6c** following S_NAr approach at 110 °C with 60–96% yields to obtain compounds **7b** and **7c** respectively. The esters **6a**, and **7b-c** were then hydrolyzed using lithium hydroxide and the crude acids **8a–c** thus obtained were converted to the ligands **1–3** using EDCI.HCl as coupling agent.

Circular Dichroism (CD) Titration Studies

Induction of a particular topology for the G4 structure by the ligands can be well-studied using CD titration experiments in the presence and in the absence of added monovalent metal cations.[13] Telomeric DNA is reported to show the well-defined antiparallel and hybrid topologies under Na^+ and K^+ buffer conditions respectively and no particular topology is shown in the absence of added metal ions or stabilizing ligands.[14,15] But, the promoter G4 DNAs are reported to form G4 structure along with the other secondary structures even in the absence of added metal cations or stabilizing ligands.[15] So the CD titration experiments without any added metal ions will help us to assess the ability of the ligands to induce any particular topology for the telomeric DNA and the ligand assisted further induction of the pre-formed G4 structure for promoter G4 DNAs.

We have performed the CD titration experiments without any added metal cations for telomeric as well as for promoter *c-MYC* and *c-KIT1* G4 DNAs with all the three ligands **1–3** (Figure 2A, 2B, Table S1 and Figure S1, Supporting Information). CD spectrum of telomeric DNA showed positive peaks around 295 nm and 255 nm, which do not correspond to any particular G4 topology (Figure 2A and Figure S1, Supporting Information). Upon titration with ligand **1**, no significant change was observed in the CD spectra and the initial peaks were retained up to the addition of 5 equivalents of ligand (Figure S1, Supporting Information). Interestingly, upon titration with ligand **2**, a positive peak around 260 nm and a negative peak around 240 nm appeared, which are the characteristic peaks for the parallel G4 topology (Figure 2A).[16] The initial peaks around

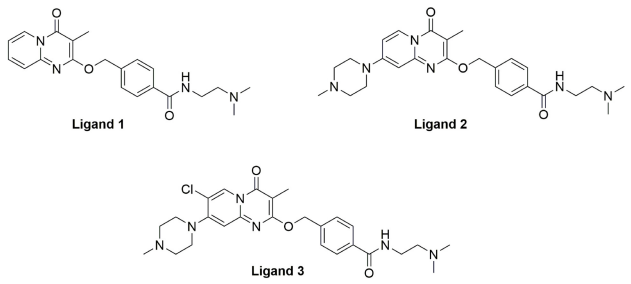

Figure 1. Structures of G4 specific ligands **1–3.**

295 nm and255 nm completely disappeared and the enhancement of new peaks around 260 nm and 240 nm has reached saturation after the addition of 10–11 equivalents of ligand **2** (Figure 2A). In the case of ligand **3**, no significant changes in the intensities of the initial peaks in the CD spectra were observed upon titration with up to 10 equivalents of ligand (Figure S1, Supporting Information). Overall, CD titration experiments with telomeric G4 DNA showed that the ligands **1** and **3** are not able to induce any particular topology for the telomeric DNA, and the ligand **2** is able to weakly induce the parallel G4 topology at high ligand concentration.

CD spectra of *c-MYC* DNA in the absence of added metal ions showed a positive peak around 260 nm, and a negative peak around 240 nm, which are the characteristic peaks for the parallel G4 topology (Figure 2B and Figure S2, Supporting Information).[16] Ligand **1** was found to be further inducing the existing parallel topology of *c-MYC* DNA, indicated by the moderate enhancement of the characteristic peaks around 260 nm and 240 nm (Figure S2, Supporting Information). But, the titration of ligands **2** and **3** with *c-MYC* DNA resulted in the strong enhancement of the characteristic peaks, indicating further induction of the pre-folded parallel G4 topology (Figure 2B and Figure S2, Supporting Information). Similar to that of *c-MYC* DNA, the CD spectrum of *c-KIT1* showed a well-defined parallel topology, indicated by the characteristic peaks around 260 nm and 240 nm (Figure S2, Supporting Information).[16] No significant change in the CD spectra was observed upon titration with the ligands **1–3**, indicating the retention of pre-folded parallel G4 structure. Overall, further induction of the pre-folded parallel G4 topology for *c-MYC* DNA and retention of the pre-folded parallel topology for *c-KIT1* were observed with the ligands.

CD Melting Studies

Ligand induced thermal stabilization of G4 DNAs can be assessed using CD spectroscopy by monitoring the ellipticity at a fixed wavelength over the temperature range of 20–95 °C.[17] CD melting experiments were carried out to evaluate the thermal stabilization properties of ligands with the telomeric and promoter *c-MYC* and *c-KIT1* G4 DNAs. Since the telomeric DNA is reported to form antiparallel and mixed hybrid G4 structures in buffer solutions containing Na^+ and K^+ ions respectively, CD melting experiments were conducted under both the Na^+ and K^+ ion conditions. The ellipticity was monitored at 295 nm and yielded $T_{1/2}$ values of 52 and 45 °C for the telomeric DNA in K^+ and Na^+ ions respectively (Figure 3A and Figure S3, Supporting Information). No significant stabilization was observed after the addition of 5 equivalents of ligands for both the antiparallel and mixed hybrid structures of telomeric G4 DNA (Table 1). In the case of mixed hybrid telomeric G4 structure, a maximum $\triangle T_{1/2}$ ~2.2 °C was observed and for the antiparallel G4 structure maximum $\triangle T_{1/2}$ ~1.5 °C was observed (Table 1). The negligible increase in the $T_{1/2}$ values reveals that the ligands are not able to stabilize the different topologies of telomeric G4 structure.

CD melting studies for the promoter *c-MYC* and *c-KIT* G4 DNAs were conducted by measuring the ellipticity at 263 nm. The salt concentrations were varied in the range of 1–10 mM,

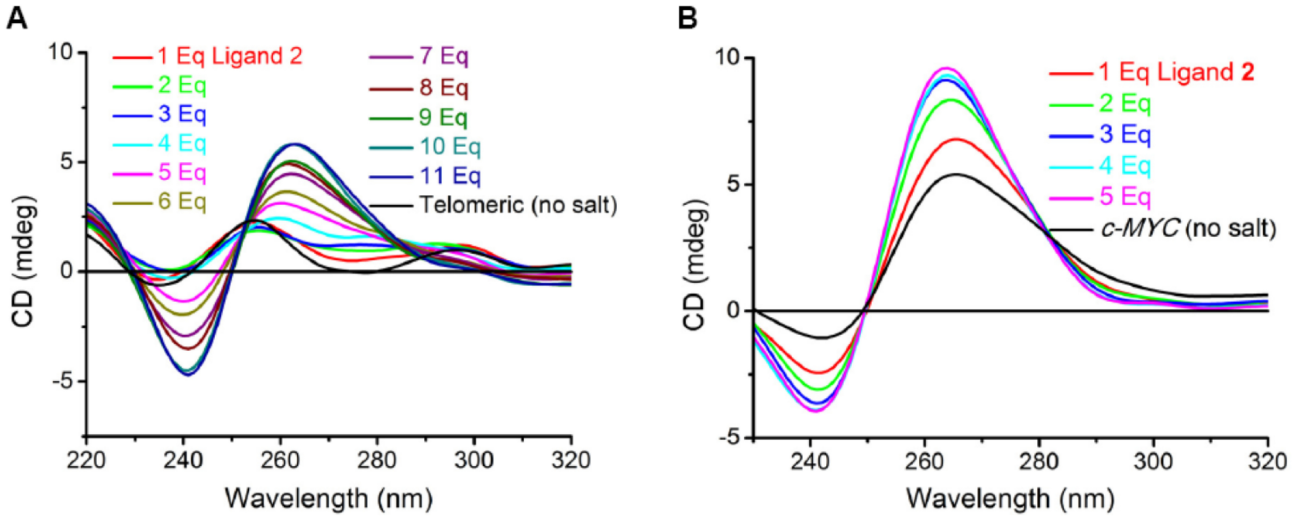

Figure 2. CD titration spectra of telomeric and *cMYC* DNAs with ligand **2** in the absence of added metal ions (12.5 μM DNA in 50 mM TrisHCl buffer, pH 7.2). (A) Telomeric DNA; and (B) *cMYC* DNA.

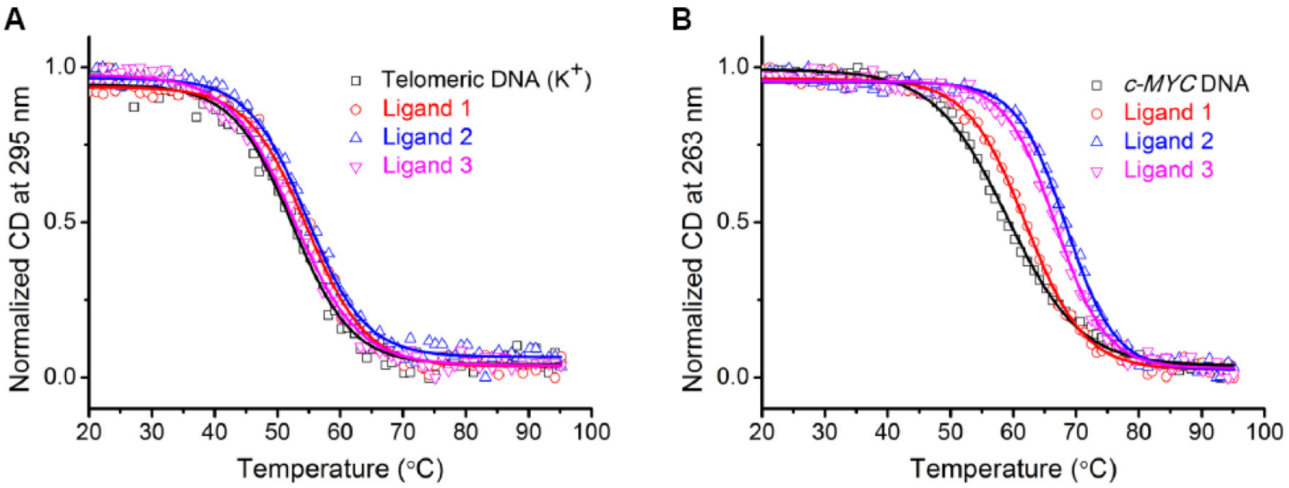

Figure 3. CD melting curves for the telomeric and the *cMYC* G4 DNAs (10 μM DNA in 10 mM lithium cacodylate buffer, pH 7.2) in the absence and in the presence of 5 equivalents of ligands. (A) Telomeric DNA (10 mM KCl and 90 mM LiCl); and (B) *cMYC* DNA (1 mM KCl and 99 mM LiCl).

Table 1. Thermal stability of G4 DNAs with the ligands measured by CD melting experiments for telomeric, *c-MYC* and *c-KIT* G4 DNAs and measured by UV melting experiments for duplex DNA

Ligands	$\triangle T_{1/2}$[a] (°C) Telomeric (K^+)	Telomeric (Na^+)	*c-MYC* (K^+)	*c-KIT1* (K^+)	*c-KIT2* (K^+)	Duplex (K^+)
1	1.4 ± 0.2	−1.3 ± 0.5	3.8 ± 0.4	-	-	−2 ± 0.4
2	2.2 ± 0.7	1.5 ± 0.7	9.1 ± 0.8	7.5 ± 0.4	4.1 ± 0.6	−1.2 ± 0.5

$\triangle T_{1/2}$ represents difference in thermal melting [$\triangle T_{1/2} = T_{1/2}$ (DNA + 5 molar equivalent ligand) - $T_{1/2}$ (DNA)]. All the experiments in KCl were carried out in 10 mM lithium cacodylate buffer pH 7.2 with 10 μM DNA concentration. $T_{1/2}$ values in the absence of ligands are 58.2 ± 0.8 °C (*c-MYC* DNA in 1 mM KCl and 99 mM LiCl); 48 ± 0.5 °C [*c-KIT1* DNA in 10 mM KCl and LiCl 90 mM); 55.5 ± 0.6 °C (*c-KIT2* DNA in 1 mM KCl and 99 mM LiCl); 52.2 ± 0.7 °C (Telomeric DNA in 10 mM KCl and 90 mM LiCl); 45.1 ± 0.3 °C (Telomeric DNA in 10 mM NaCl, 90 mM LiCl, and 10 mM sodium cacodylate buffer, pH 7.2); and 64.1 ± 0.4 °C (Duplex DNA in 10 mM KCl and 90 mM LiCl). $\triangle T_{1/2}$ values are reported as the average values with standard deviations from 3 independent experiments.

depending on the stability of the G4 structures to keep the melting temperature in the range of 40–60 °C. This provides a sufficient analysis window to monitor the ligand induced stabilization of G4 DNAs. For the *c-MYC* DNA, the $T_{1/2}$ value was moderately increased after the addition of 5 equivalents of ligands (Figure 3B). Ligand **1** was found to be weakly stabilizing the parallel *c-MYC* G4 DNA with $\triangle T_{1/2}$ ~3.8 °C, whereas the other two ligands **2** and **3** showed moderate stabilization with $\triangle T_{1/2}$ ~9.1 and 8.8 °C, respectively (Figure 3B and Table 1). The ligands **2** and **3** were selected for further studies to assess the ligand-G4 DNA interaction due to their increased stabilization with the *c-MYC* G4 DNA. For the *c-KIT1* G4 DNA, the $T_{1/2}$ value was increased with the ligands **1** and **2**, yielding $\triangle T_{1/2}$ ~7.5 and 12 °C respectively (Figure S3, Supporting Information and Table 1). But, in the case of *c-KIT2* G4 DNA both the ligands imparted weak stabilization, yielding $\triangle T_{1/2}$ ~4.1 and 5.5 °C for ligand **2** and **3**respectively (Figure S3, Supporting Information and Table 1).

Overall, CD melting studies revealed the preferential stabilization of parallel topology of promoter *c-MYC* and *c-KIT* G4 DNAs by the ligands **1–3** over the different topologies of telomeric G4 DNA. We have also carried out CD melting experiments with duplex DNAs in order to address the selectivity of these ligands with duplex DNAs. Unfortunately, we were not able to observe accurate and reliable CD melting curves after incubating with the ligands. As an alternative, we have carried out UV melting experiments by monitoring the absorbance at 260 nm. No significant duplex stabilization was observed after incubation with 5 equivalents of the ligands (Table 1 and Figure S4, Supporting Information).

Isothermal Titration Calorimetry (ITC) Studies

The thermodynamic parameters for the ligand-DNA interactions can be derived using ITC experiments.[18] Ligand **2** was selected for the ITC experiments due to its G4 stabilization properties and increased solubility in water. Since the *c-MYC* G4 DNA is extensively studied among the parallel promoter G4 DNAs, ITC experiments were performed by taking *c-MYC* DNA as an example for parallel promoter G4 DNAs. To address the preferential stabilization of promoter G4 DNAs over telomeric and the selectivity over duplex DNAs, ITC experiments were carried out with telomeric G4 and duplex DNAs as well (Table 2, Figure 4, and Figure S5, Supporting Information). The isotherms were fitted by using sequential model to extract the binding constant and the thermodynamic parameters for the ligand-

Table 2. Thermodynamic parameters obtained from ITC experiments for the interaction of ligand **2** with *c-MYC* G4 DNAs at 25 °C

$K_1 \times 10^5$	$\triangle H_1$	$T\triangle S_1$	$K_2 \times 10^5$	$\triangle H_2$	$T\triangle S_2$	$K_3 \times 10^4$	$\triangle H_3$	$T\triangle S_3$
				c-MYC G4 DNA				
4.9 ± 0.1	−9.4 ± 0.1	−0.1	1 ± 0.1	−8.9 ± 0.1	−0.2	1.3 ± 0.02	−19 ± 0.3	−1.2
				Telomeric G4 DNA				
0.1 ± 0.01	−23.2 ± 1	−1.5	0.3 ± 0.03	9.5 ± 1	1.3	-	-	-
				Duplex DNA				
0.2 ± 0.01	−12.6 ± 0.4	−0.6	0.08	−20.7 ± 1	−1.3	0.4 ± 0.02	34.1 ± 2	3.3

Best fit parameters obtained by sequential binding model with $Chi^2 = 3192$, n = 3 for the *c-MYC* G4 DNA, $Chi^2 = 13090$, n = 2 for the telomeric G4 DNA, and $Chi^2 = 7028$, n = 3 for Duplex DNA. *K* values are in M^{-1} and $\triangle H$, $T\triangle S$ values are in kcal/mol.

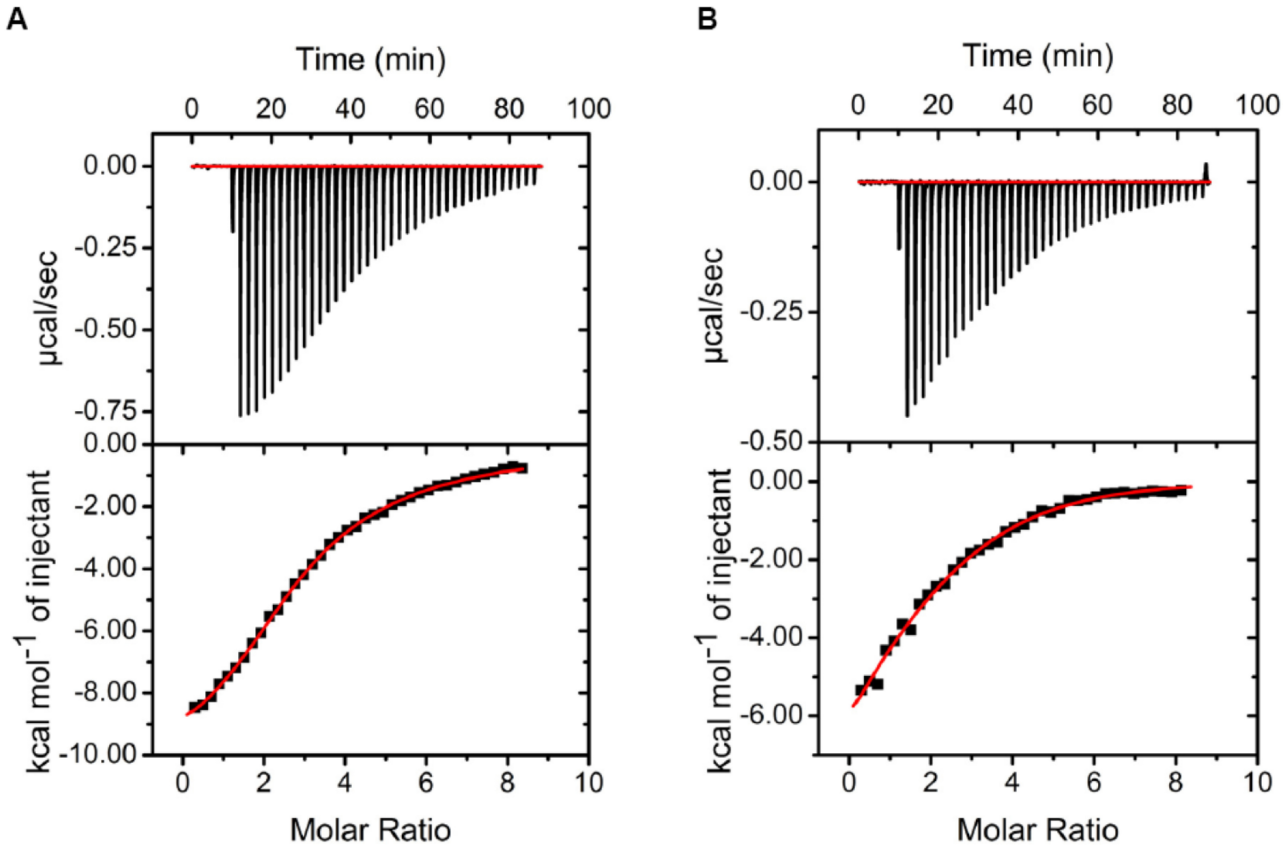

Figure 4. ITC profiles for the interaction of ligand **2** with *c-MYC* and telomeric G4 DNA (25 µM DNA in 100 mM KCl and 10 mM lithium cacodylate buffer, pH 7.2). (A) *c-MYC* DNA; and (B) Telomeric DNA. Raw data shown in upper panel and curve fit using sequential binding model in the bottom panel with $Chi^2 = 3192$, n = 3 and $Chi^2 = 13090$, n = 2 for *c-MYC* and telomeric G4 DNAs respectively.

DNA interaction. As expected, ligand **2** showed moderate binding interaction with the *c-MYC* G4 DNA, which is indicated by the binding constant values, $K_1 = 4.9 \times 10^5$ and $K_2 = 1 \times 10^5$ M^{-1} (Figure 4A, Table 2).

Moreover, the exothermic interaction was observed for the ligand **2** with the *c-MYC* G4 DNA, which is reflected in the large negative enthalpy change (Figure 4A and Table 2,). ITC experiments with telomeric and duplex DNAs yielded binding constant values, $K_1 = 1 \times 10^4$ M^{-1} for telomeric and $K_1 = 2 \times 10^4$ M^{-1} for duplex DNAs, indicating relatively weak binding of the ligand **2** (Table 2, Figure 4B and Figure S5, Supporting Information). These data show that ligand **2** has moderate affinity to the *c-MYC* G4 DNA with ~49-fold selectivity over the telomeric G4 DNA and ~25-fold selectivity over the duplex DNAs (Table 2). Overall, the results from the ITC experiments are consistent with those from the CD spectroscopic studies, and confirm the preferential stabilization of parallel topology of *c-MYC* G4 DNAs over telomeric and duplex DNAs by the ligand **2.**

Molecular Modeling and Dynamics Studies

To understand the interactions governing the recognition of G4 DNAs by the ligand **2,** molecular modeling and dynamics simulations were carried out with c-*MYC* and c-*KIT1* G4 DNA structures. The energy optimized ligand **2** at HF/6-31 + G**

level (Figure S6 and S7, Supporting Information) was docked with c-*MYC* (PDB entry: 2L7V)[19] and c-*KIT1* (PDB entry: 2O3M)[20] G4 DNA structures using AutoDock 4.2.[21] Docking results revealed that ligand **2** prefers binding at the 5′-end of the c-*MYC* DNA, and at the 3′-end of the c-*KIT1* DNA. Based on these results, a total of 500 ns unrestrained dynamics were carried out for both the complexes using GPU accelerated version of PMEMD in AMBER 14.[22,23]

To understand the conformational stability of the G4 DNAs and the conformational flexibility of the ligand **2** upon binding to G4 DNA, the root mean square deviation (RMSD) values of heavy atoms of the ligand, backbone and G-quartets were calculated separately with respect to the first frame. RMSD values of G-quartets showed nominal fluctuations indicating the stabilizing effect of the ligand **2** (Figure 5A and 5C). The

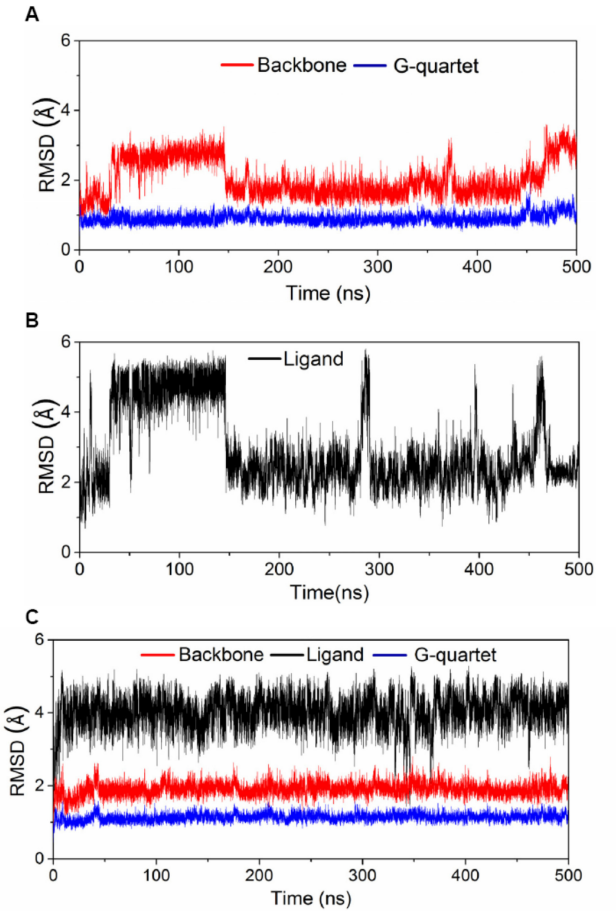

Figure 5. Time dependent RMSD values of ligand **2** bound to c-*MYC* and c-*KIT1* complexes. Each 5th snapshot was considered and a total of 50,000 frames were used for the calculation. Values were calculated using cpptraj module in AMBER14 (A) and (B) c-*MYC*-ligand **2** complex; and (C) c-*KIT1*-ligand **2** complex.

RMSD graph of the c-*MYC* G4 DNA backbone showed fluctuations, which can be attributed to the flexibility of flanking nucleotides (Figure 5 A). This is also evident from the per-nucleotide-root mean square fluctuation (RMSF) values (Figure S8). Nucleotides 1–3 of c-*MYC* G4 DNA have shown fluctuations >1.8 Å with respect to starting structure, whereas G-quartet forming nucleotides showed <1.0 Å fluctuations. The c-*KIT1* G4 DNA backbone showed stable RMSD (Figure 5C). Ligand **2** showed considerable fluctuations owing to its flexible structure in both c-*MYC* and c-*KIT1* complexes (Figure 5A and 5B). Percentage occupancies of the Hoogsteen H-bonds were calculated for G-quartets and were found to be $>96\%$ in both complexes.

The 500 ns dynamics of both the complexes were clustered into 5 ensembles; each ensemble having a representative structure. The complex with c-*MYC* G4 DNA showed two major ensembles each one contributing for ~70% and ~22% of the total simulation time. The representative structures of two ensembles of c-*MYC* complex were superimposed to check the differences. Major differences were observed in the orientations of nucleotides dT1 and dG2, and also in the conformation of ligand (Figure S9A, Supporting Information). Complex with c-*KIT1* G4 DNA also showed two major ensembles contributing for ~50% and 45% of the simulation time. In the case of c-*KIT1* as well, the representative structures were very similar with only major difference in the orientation of nucleotide dC8 (Figure S9B, Supporting Information).

Representative snapshots of major clusters of c-*MYC* and c-*KIT1* dynamics are shown in the Figure 6. Stacking interactions are the major stabilizing forces that are present between ligand **2** and c-*MYC* G4 DNA. The flanking nucleotide dG2 stacks on ligand surface while dG1 stacks on dG2. Ligand is sandwiched between dG2 and G-quartet (Figure 6A and 6B). The RMSF value observed for the ligand is 2.7 Å, which shows that the ligand has moved to some extent compared to the starting structure. No significant intermolecular H-bonds between ligand **2** and c-*MYC* G4 DNA were observed during the MD simulations. In the case of c-*KIT1*-ligand **2** complex, apart from stacking interactions, one major H-bond between O3 of the ligand **2** and N–H of the nucleotide dG19 (Figure 6D and Figure S10, Supporting Information) was present for ~74% of the total simulation time with an average distance and angle of 2.8 Å and 155° respectively. The RMSF value observed for the ligand is 1.8 Å, which shows that there is no appreciable change in the binding conformation compared to starting structure (Figure 5C). However, it was observed during dynamics that the ligand replaces residues dA15 and dG19 which stack on G-quartet. (Figure S11, Supporting Information).

To probe the preferential binding of ligand **2,** docking and dynamics have been performed with the physiologically relevant hybrid-2 telomeric G-quadruplex (PDB entry: 2JPZ[24]). During the docking, the ligand **2** was found to be bound to 5′ end with partial access to G-quartet and to the groove. During the course of dynamics, the DNA backbone changed to accommodate the ligand and the ligand formed stacking interactions with the loop nucleotides. Although the G-quartet was partially accessible to the ligand, it couldn't replace the end-stacking nucleotides. Eventually, the ligand lost it's binding with hybrid-2 G-quadruplex at 76ns (Figure S12, Supporting Information). These results show why the ligand **2** is not able to

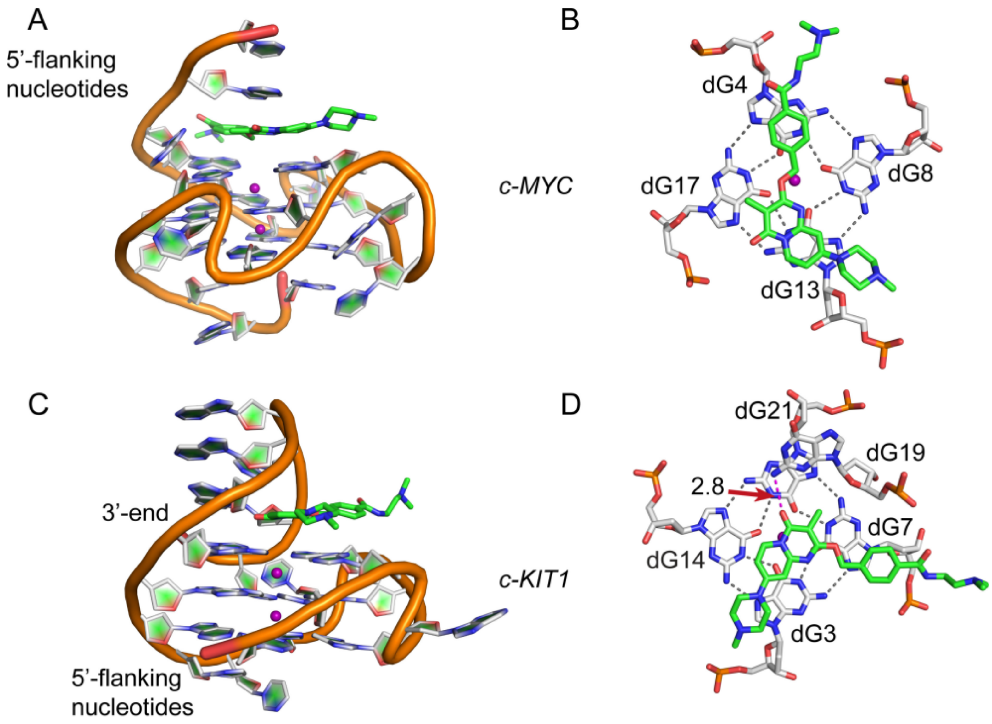

Figure 6. Representative snapshots of major clusters of ligand bound *c-MYC* and *c-KIT1* G4 DNAs. (A) Ligand bound to the 5′-end face of the *c-MYC* G4 DNA (side view); (B) axial view of ligand stacked on the *c-MYC* G4 DNA quartet; (C) Ligand bound to 3′-end of *c-KIT1* G4 DNA (side view); and (D) axial view of ligand stacked on *c-KIT1* G4 DNA quartet. Gray dotted lines represent the Hoogsteen H-bonds. Magenta dotted lines represent the H-bond. K^+ ions are shown as purple spheres. The distance is mentioned Å. Carbon atoms of DNA are represented using white and carbon atoms of ligand are represented using green, nitrogen atoms using blue, oxygen atoms using red and phosphorus using orange-red.

strongly stabilize telomeric G4 structure as revealed in the biophysical studies.

The binding energy calculations were performed from the last 20 ns using MM-PBSA[25] in AMBER14. The *c-MYC* G4 DNA displayed more negative binding free energy compared to *c-KIT1* G4 DNA (Table 3 and Table S2, Supporting Information).

Table 3. Binding free energy values of *c-KIT1* and *c-MYC* G4 complexes.

Structures	$\triangle H$	$T\triangle S$	$\triangle G = \triangle H - T\triangle S$
c-MYC (2 L7 V)	-41.74 ± 4.52	-19.16 ± 4.48	-22.57 ± 6.50
c-KIT1 (2O3 M)	-36.12 ± 3.96	-21.92 ± 4.37	-11.80 ± 5.80

Enthalpy values are obtained through MM-PBSA[25] method and entropy values are calculated using nmode calculations. All values are reported in kcal mol^{-1}. The values are calculated for 2000 snapshots over last 20 ns of MD simulation.

The data show that the loss of entropy upon complexation is similar in both the cases but the gain in enthalpy was greater for the *c-MYC* G4 DNA leading to slightly higher affinity toward *c-MYC* G4 DNA.

Conclusions

G4 stabilizing ligands harboring drug like properties, which have selectivity and specificity toward a particular G4 topology can be harnessed as anticancer agents. In this direction, we have designed and synthesized potential drug-like G4 stabilizing ligands, which are the benzamide derivatives of pyridopyrimidinone scaffold. Results from the biophysical studies like CD melting and ITC confirms the preferential stabilization of the ligands with the *c-MYC* and *c-KIT* promoter G4 DNAs with parallel topologies over the various topologies of telomeric G4 and duplex DNAs. Molecular modeling and dynamics studies shed light into the end stacking mode of interactions between the ligand and the promoter *c-MYC* and *c-KIT1* G4 DNA structures and it's preferential binding over the teloemeric G4 DNA. Overall, the preferential stabilization of promoter *c-MYC* and *c-KIT1* G4 DNA structures along with the simplicity in the molecular structure and the increased aqueous solubility project the new scaffolds for future SAR and further biological studies.

Acknowledgments

C.R. sincerely acknowledges TCGLS for the opportunity to pursue this work. C.R. and M.K. are thankful to analytical team at TCGLS for the structural elucidation and discussion on the spectral data. Computer centre at IIT Bombay is gratefully acknowledged for providing high performance computing facilities. We are thankful to the central facility supported by IRCC-IIT Bombay for MALDI-MS facility. We are also thankful to Dr. Ruchi Anand for providing access to her laboratory facilities. This work is financially supported by grants from the Department of Biotechnology (DBT)-Government of India (Pilot Project Grants for Young Investigators in Cancer Biology, Grant No: 6242-P4/RGCB/PMD/DBT/PKPI/2015, to P.I.P. and from Science and Engineering Research Board (SERB-DST)-Government of India (Grant No. EMR/2016/003268) to P.I.P. D.K.V. and SPPP thank Council of Scientific and Industrial Research (CSIR), India for the Ph.D. fellowships. P.B. thanks Department of Science and Technology (DST) for the Inspire Fellowship.

Conflict of Interest

The authors declare no conflict of interest.

Keywords: anti-cancer · drug-design · G-quadruplexes · nucleic acids · pyridopyrimidinone scaffold

[1] L. H. Hurley, *Nat. Rev. Cancer* **2002**, *2*, 188 – 200.
[2] S. Balasubramanian, L. H. Hurley, S. Neidle, *Nat. Rev. Drug Discovery* **2011**, *10*, 261 – 275.
[3] G. W. Collie, G. N. Parkinson, *Chem. Soc. Rev.* **2011**, *40*, 5867 – 5892.
[4] S. M. Haider, S. Neidle, G. N. Parkinson, *Biochimie* **2011**, *93*, 1239 – 1251.
[5] M. L. Bochman, K. Paeschke, V. A. Zakian, *Nat. Rev. Genet.* **2012**, *13*, 770 – 780.
[6] S. Zhang, Y. Wu, W. Zhang, *ChemMedChem* **2014**, *9*, 899 – 911.
[7] S. Neidle, *J. Med. Chem.* **2016**, *59*, 5987 – 6011.
[8] K. V. Diveshkumar, S. Sakrikar, S. Harikrishna, V. Dhamodharan, P. I. Pradeepkumar, *ChemMedChem* **2014**, *9*, 2754 – 2765.
[9] V. Dhamodharan, S. Harikrishna, A. C. Bhasikuttan, P. I. Pradeepkumar, *ACS Chem. Biol.* **2015**, *10*, 821 – 833.
[10] S. P. Priyadarshinee Pany, P. Bommisetti, K. V. Diveshkumar, P. I. Pradeepkumar, *Org. Biomol. Chem.* **2016**, *14*, 5779 – 5793.
[11] K. V. Diveshkumar, S. Sakrikar, F. Rosu, S. Harikrishna, V. Gabelica, P. I. Pradeepkumar, *Biochemistry* **2016**, *55*, 3571 – 3585.
[12] C. Plüg, B. Wallfisch, H. G. Andersen, P. V. Bernhardt, L–J. Baker, G. R. Clark, M. W. Wong, C. Wentrup, *J. Chem. Soc. Perkin Trans.* **2000**, *2*, 2096 – 2108.
[13] S. Paramasivan, I. Rujan, H. P. Bolton, *Methods* **2007**, *43*, 324 – 331.
[14] A. Ambrus, D. Chen, J. Dai, T. Bialis, R. A. Jones, D. Yang, *Nucleic Acids Res.* **2006**, *34*, 2723 – 2735.
[15] E. M. Rezler, J. Seenisamy, S. Bashyam, K. Mu-Yong, E. White, W. D. Wilson, L. H. Hurley, *J. Am. Chem. Soc.* **2005**, *127*, 9439 – 9447.
[16] J. Dash, P. S. , Shirude, S. D. Hsu, S. Balasubramanian, *J. Am. Chem. Soc.* **2008**, *130*, 15950 – 15956.
[17] A. Guedin, L. Lacroix, J. L. Mergny, *Methods Mol. Biol.* **2010**, *613*, 25 – 35.
[18] M. W. Freyer, E. A. Lewis, *Methods Cell Biol.* **2008**, *84*, 79 – 113.
[19] J. Dai, M. Carver, L. H. Hurley, D. Yang, *J. Am. Chem. Soc.* **2011**, *133*, 17673 – 17680.
[20] A. T. Phan, V. Kuryavyi, S. Burge, S. Neidle, D. J. Patel, *J. Am. Chem. Soc.* **2007**, *129*, 4386 – 4392.
[21] G. M. Morris, R. Huey, W. Lindstrom, M. F. Sanner, R. K. Belew, D. S. Goodsell, A. J. Olson, *J. Comput. Chem.* **2009**, *30*, 2785 – 2791.
[22] a) R. Salomon-Ferrer, A. W. Götz, D. Poole, S. Le Grand, R. C. Walker, *J. Chem. Theory Comput.* **2013**, *9*, 3878 – 3888; b) A. W. Götz, M. J. Williamson, D. Xu, D. Poole, S. Le Grand, R. C. Walker, *J. Chem. Theory Comput.* **2012**, *8*, 1542 – 1555; c) S. Le Grand, A. W. Götz, R. C. Walker, *Comput. Phys. Commun.* **2013**, *184*, 374 – 380.
[23] D. A. Case, T. A. Darden, T. E. Cheatham, C. L. Simmerling, J. Wang, R. E. Duke, R. Luo, R. C. Walker, W. Zhang, K. M. Merz, B. Roberts, B. Wang, S. Hayik, A. Roitberg, G. Seabra, I. Kolossváry, K. F. Wong, F. Paesani, J. Vanicek, J. Liu, X. Wu, S. R. Brozell, T. Steinbrecher, H. Gohlke, Q. Cai, X. Ye, J. Wang, M. J. Hsieh, G. Cui, D. R. Roe, D. H. Mathews, M. G. Seetin, C. Sagui, V. Babin, S. Gusarov, A. Kovalenko, P. A. Kollman, *AMBER 14*, **2014**.
[24] J. Dai, M. Carver, C. Punchihewa, R. A. Jones, D. Yang, *Nucleic Acids Res.* **2007**, *35*, 4927 – 4940.
[25] P.A. Kollman, I. Massova, C. Reyes, B. Kuhn, S. Huo, L. Chong, M. Lee, T. Lee, Y. Duan, W. Wang, O. Donini, P. Cieplak, J. Srinivasan, D. A. Case, T. E. Cheatham, *Acc. Chem. Res.* **2000**, *33*, 889 – 897.

Submitted: March 29, 2017
Revised: June 14, 2017
Accepted: June 19, 2017

ChemistrySELECT

Supporting Information

Pyridopyrimidinone Derivatives as DNAG-Quadruplex-Stabilizing Agents: Design, Synthesis and Biophysical Studies

Rajesh Malhotra[+], Chhanda Rarhi[+], K. V. Diveshkumar[+], P. Bommisetti, Sushree Prangya P. Pany, Subho Roy, P. I. Pradeepkumar,* and Mrinalkanti Kundu*

Supporting Information

TABLE OF CONTENTS

Figure S1 CD spectra of ligands with telomeric G4 DNA in the absence of added metal ions... Page S4

Figure S2 CD spectra of ligands with *c-MYC* and *c-KIT1* G4 DNAs in the absence of added metal ions..... Page S5

Figure S3 CD melting curves of ligands with telomeric and promoter G4 DNAs..... Page S6

Figure S4 UV melting curves of ligands with duplex DNA ..... Page S6

Figure S5 ITC profiles of ligand **2** with duplex DNA..... Page S7

Figure S6 Optimized structure of ligand used for docking ..... Page S7

Figure S7 Various stages of ligand optimization process ..... Page S8

Figure S8 Per-nucleotide RMSF values of c-*MYC* and c-*KIT1* G4 DNAs ..... Page S9

Figure S9 Comparison of representative structures of ensembles of c-*MYC* and c-*KIT1*-ligand **2** complexes ..... Page S10

Figure S10 H-bonds between ligand **2** and c-*KIT1* G4 DNA..... Page S11

Figure S11 Reorientation of ligand **2** during dynamics of c-*KIT1* complex ..... Page S11

Figure S12 Reorientation of ligand **2** during dynamics of telomeric hybrid – 2 complex..... Page S12

Table S1 Oligonucleotides used for biophysical studies..... Page S13

Table S2 Binding free energy components of the c-*MYC* and c-*KIT1* G4 DNA -ligand **2** Complexes……Page S13

Experimental section ……Page S14-22

^{1}H NMR spectrum of compound **6a**.....Page S23

^{13}C NMR spectrum of compound **6a**.....Page S24

^{1}H NMR spectrum of compound **1**.....Page S25

^{13}C NMR spectrum of compound **1**.....Page S26

APT spectrum of compound **1**.....Page S27

HPLC chromatogram of compound **1** .....Page S28

^{1}H NMR spectrum of compound **5b**.....Page S29

^{13}C NMR spectrum of compound **5b**.....Page S30

APT spectrum of compound **5b** .....Page S31

^{1}H NMR spectrum of compound **6b**.....Page S32

^{13}C NMR spectrum of compound **6b**.....Page S33

APT spectrum of compound **6b** ..... Page S34

^{1}H NMR spectrum of compound **7b** ..... Page S35

^{13}C NMR spectrum of compound **7b** ..... Page S36

^{1}H NMR spectrum of compound **2** ..... Page S37

^{13}C NMR spectrum of compound **2** ..... Page S38

HPLC chromatogram of compound **2** ..... Page S39

^{1}H NMR spectrum of compound **5c** ..... Page S40

^{13}C NMR spectrum of compound **5c** ..... Page S41

^{1}H NMR spectrum of compound **6c** ..... Page S42

^{13}C NMR spectrum of compound **6c** ..... Page S43

^{1}H NMR spectrum of compound **7c** ..... Page S44

^{13}C NMR spectrum of compound **7c** ..... Page S45

^{1}H NMR spectrum of compound **8c** ..... Page S46

^{13}C NMR spectrum of compound **8c** ..... Page S47

^{1}H NMR spectrum of compound **3** ..... Page S48

^{13}C NMR spectrum of compound **3** ..... Page S49

HPLC chromatogram of compound **3** ..... Page S50

References ..... Page S51

CD spectra of ligands with telomeric G4 DNA in the absence of added metal ions

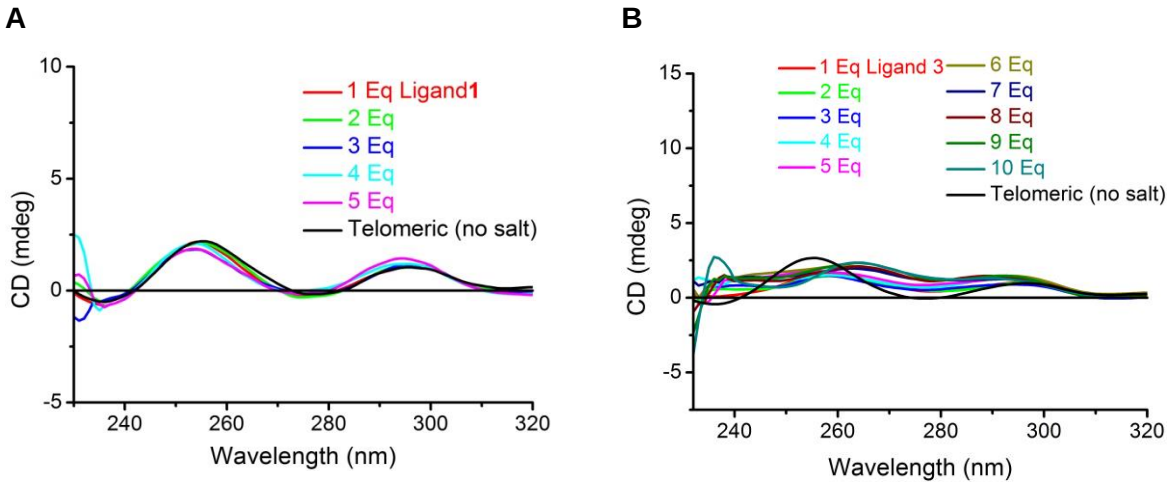

Figure S1. CD titration spectra of ligands with telomeric G4 DNA (12.5 µM DNA in 50 mM Tris, pH 7.2) in the absence of added metal ions. (A) Ligand **1**; and (B) Ligand **3**.

CD spectra of ligands with *c-MYC* and *c-KIT1* G4 DNAs in the absence of added metal ions

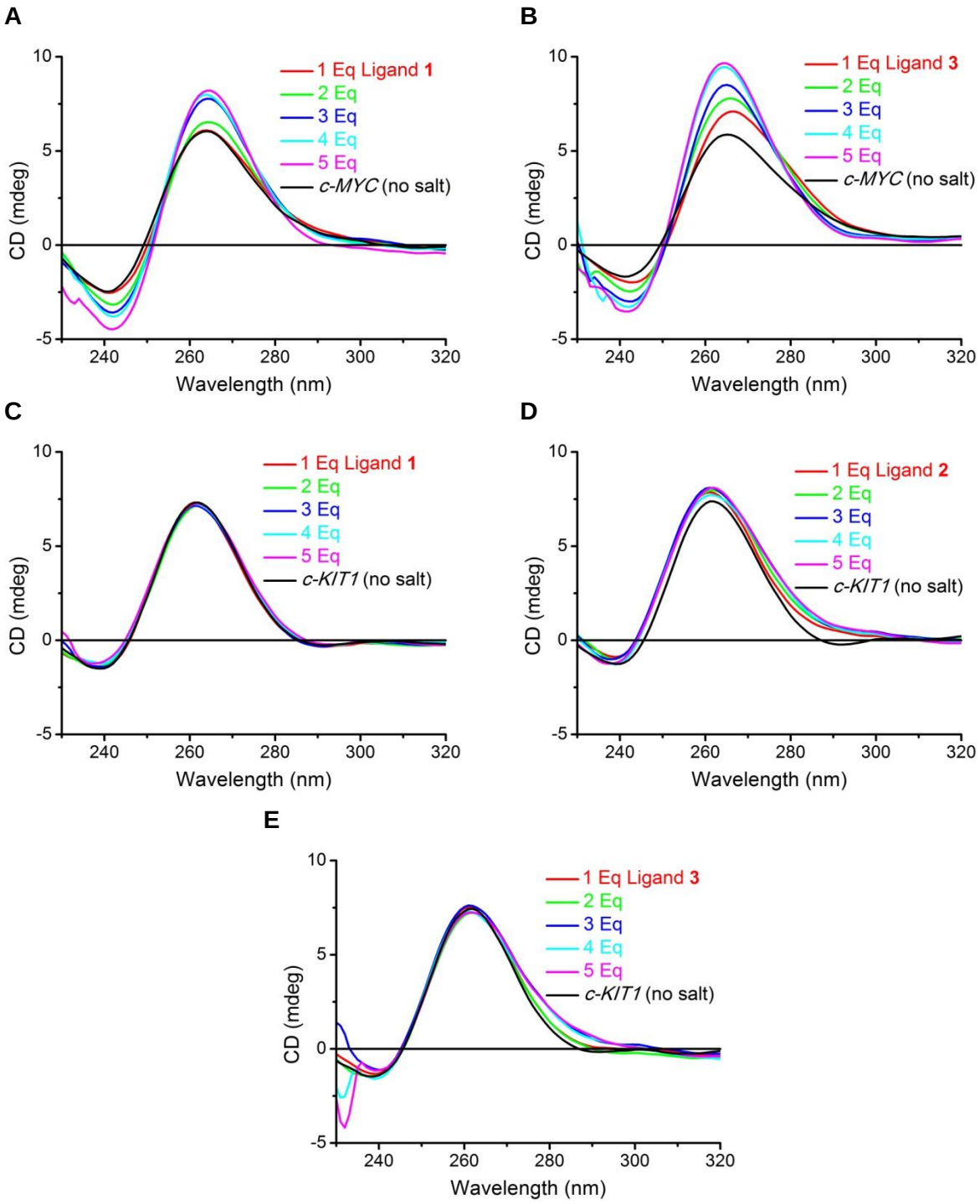

Figure S2. CD titration spectra of ligands with *c-MYC* and *c-KIT1* DNAs (12.5 µM DNA in 50 mM Tris, pH 7.2) in the absence of added metal ions. (A) *c-MYC* DNA with ligand **1**; (B) *c-MYC* DNA with ligand **3** (C) *c-KIT1* DNA with ligand **1**; (D) *c-KIT1* DNA with ligand **2**; and (E) *c-KIT1* DNA with ligand **3**.

CD melting curves of ligands with telomeric and promoter G4 DNAs

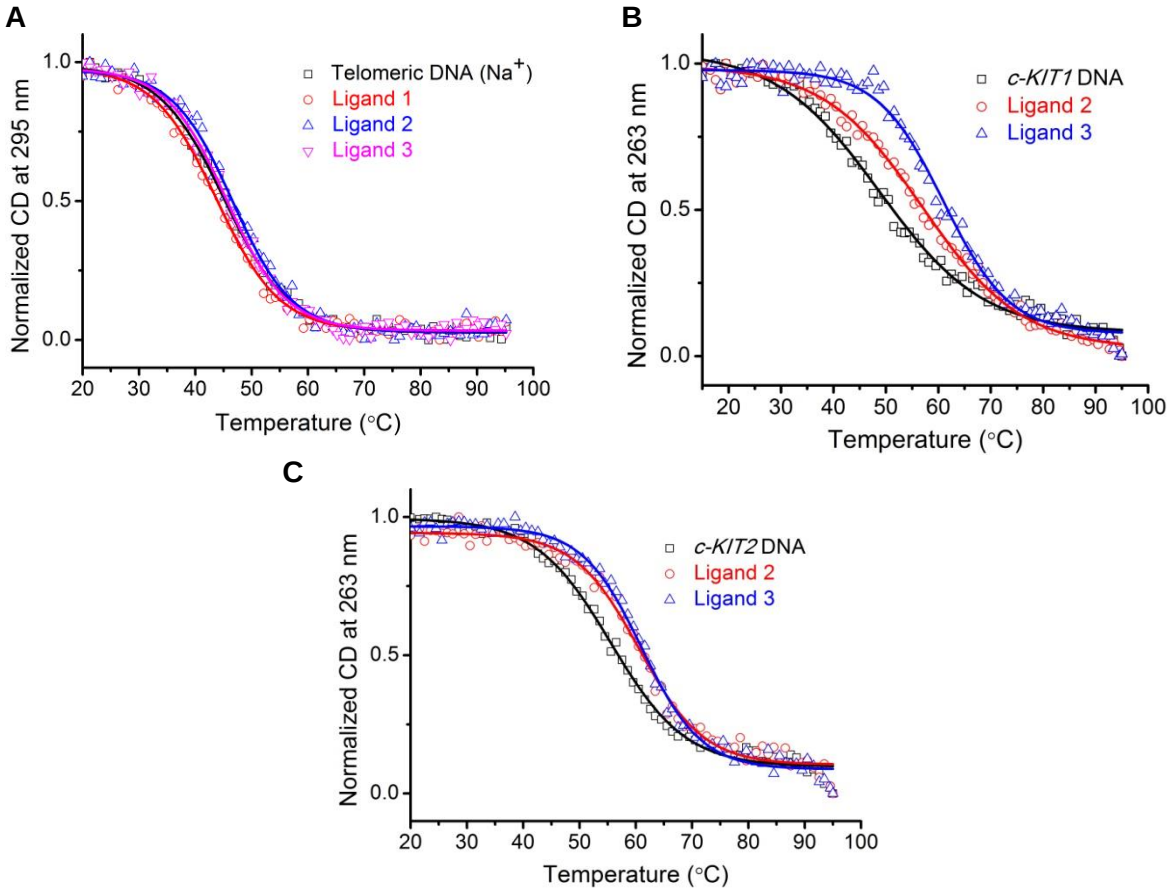

Figure S3: CD melting curves of telomeric and promoter G4 DNAs (10 μM in 10 mM lithium or sodium cacodylate buffer, pH 7.2). (A) Telomeric DNA, (10 mM NaCl, 90 mM LiCl, and sodium cacodylate buffer, pH 7.2); (B) *c-KIT1* DNA, (10 mM KCl and 90 mM LiCl); and (C) *c-KIT2* DNA, (1 mM KCl and 99 mM LiCl)

UV melting curves of ligands with duplex DNA

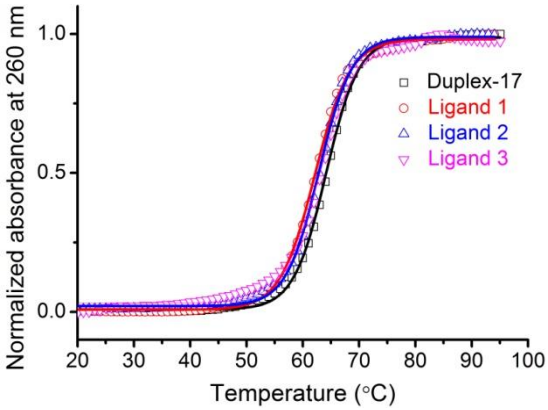

Figure S4: UV melting curves for the ligands with duplex DNA (5 μM in 10 mM KCl, 90 mM LiCl, and lithium cacodylate buffer, pH 7.2). The $T_{1/2}$ value for the duplex DNA was 64.1 ± 0.2 °C and the $\Delta T_{1/2}$ values were −2 ± 0.5 °C, −1.3 ± 0.2 °C, and −1 ± 0.6 °C with the ligands **1**, **2**, and **3**.

ITC profiles of ligand 2 with duplex DNA

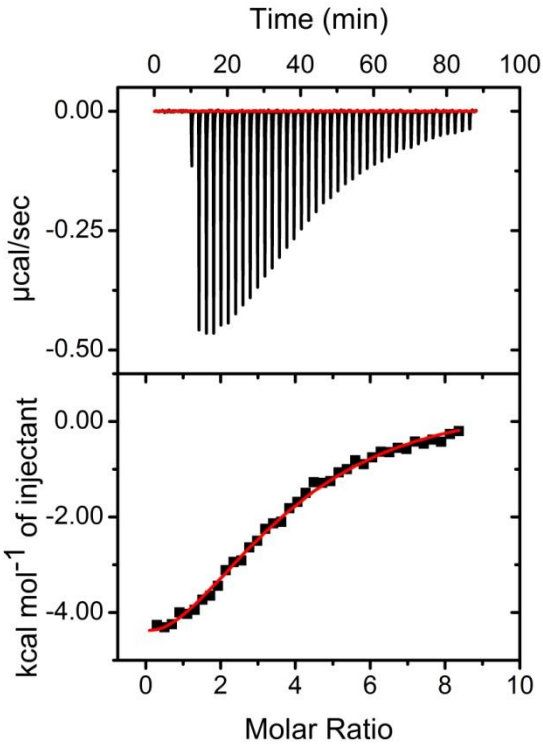

Figure S5. ITC profiles for the interaction of ligand **2** with duplex DNA (25 µM DNA in 100 mM KCl and 10 mM lithium cacodylate buffer, pH 7.2). Raw data shown in upper panel and curve fit using sequential binding model in the bottom panel with Chi^2 = 7028 and n = 3.

Optimized structure of ligand 2 used for docking

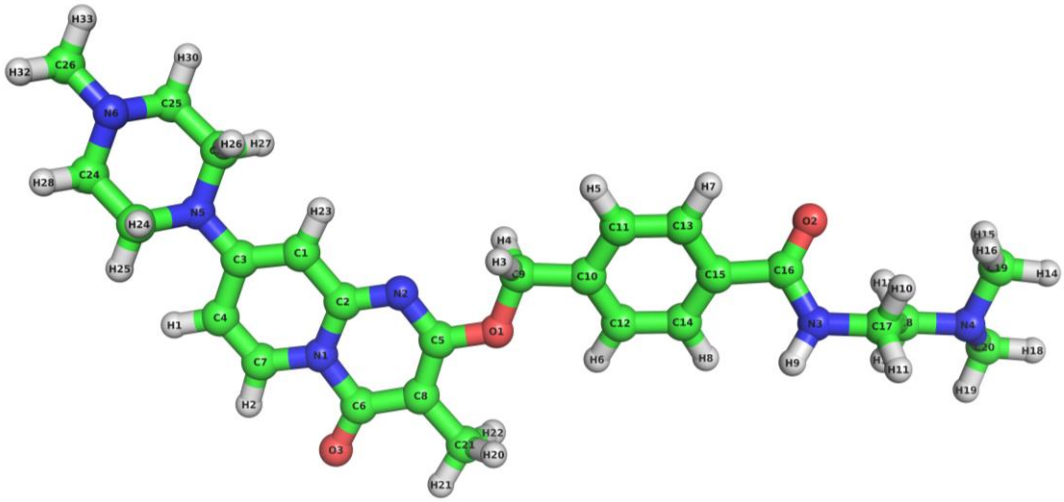

Figure S6. The optimized structure of ligand **2** which was used for docking. The ligand was optimized at HF/6-31+G** theory level. Carbon atoms are represented using green, oxygen atoms using red, nitrogen atoms using blue and hydrogen atoms using light gray.

Various stages of ligand 2 optimization process

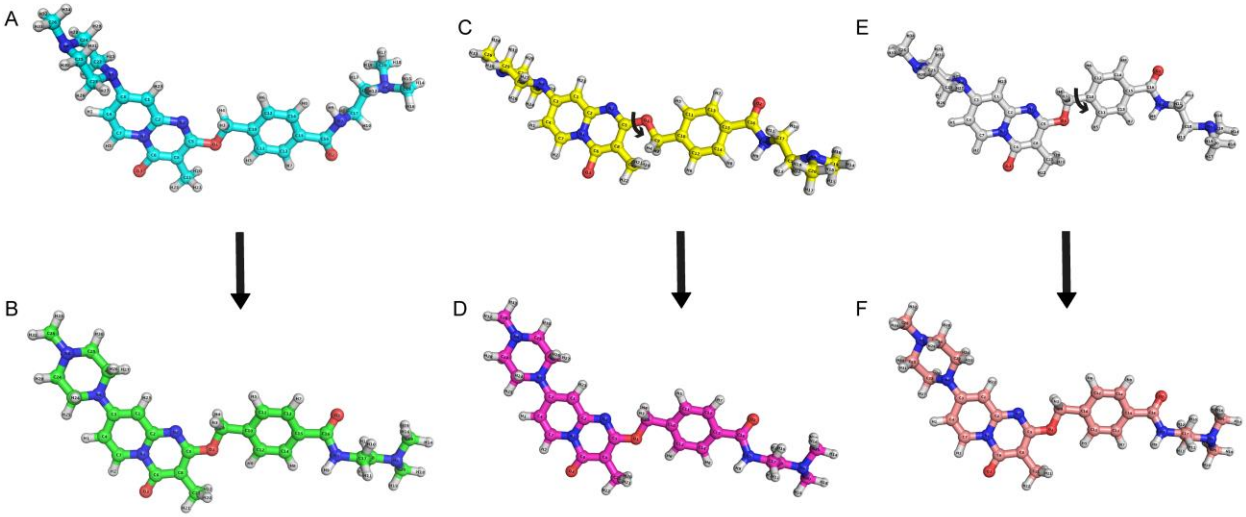

Figure S7. Torsions considered for optimization of ligand **2**. Initially the ligand was built in Gauss view without any bias and optimized at HF/6-31+G** level. This led to the structure as shown in B. Later, the torsion shown using an arrow in C was rotated such that C14 was in close proximity with C26 atom (compare with structure A). This conformation was eventually optimized to a similar structure as shown in B. Similarly, the torsion shown using an arrow in E was rotated such that O2 was pointing upwards (compare with structure A). This conformation too eventually optimized to a similar structure as B. Also structures B,D,F have similar energies. Therefore, the structure B was used for docking. Methyl and phenyl substituents on the 1,4 positions of piperazine ring are placed in equatorial positions in order to avoid the 1,3 axial steric clashes of these groups with other hydrogens. Carbon atoms are represented using cyan in A, green in B, yellow in C, magenta in D, white in E and brow-red in F. Nitrogen atoms are represented in blue and oxygen atoms in red.

Per-nucleotide RMSF values of c-*MYC* and c-*KIT1* G4 DNAs

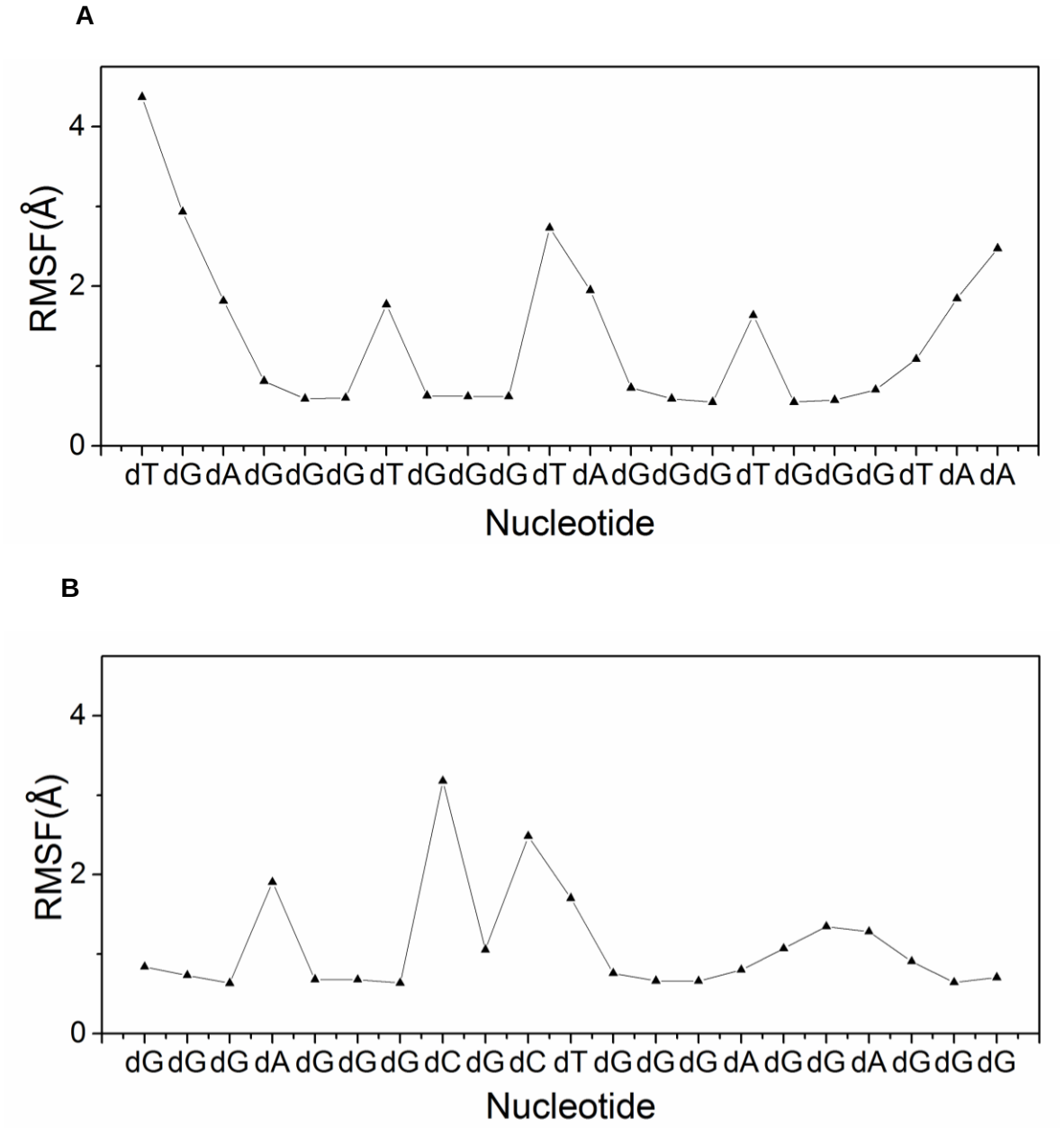

Figure S8. Per-nucleotide-RMSF values of individual nucleotides. (A) c-*MYC* G4 DNA; (B) c-*KIT*1 G4 DNA. The graphs are plotted as fluctuations against the nucleotide number. The sequence on the X-axis is written in 5'-3' direction. Every 5th frame was considered, and a total of 50,000 frames were considered for the calculation. The values are calculated using cpptraj module in AMBER14.

Comparison of representative structures of ensembles of c-*MYC* and c-*KIT1* –ligand 2 complexes

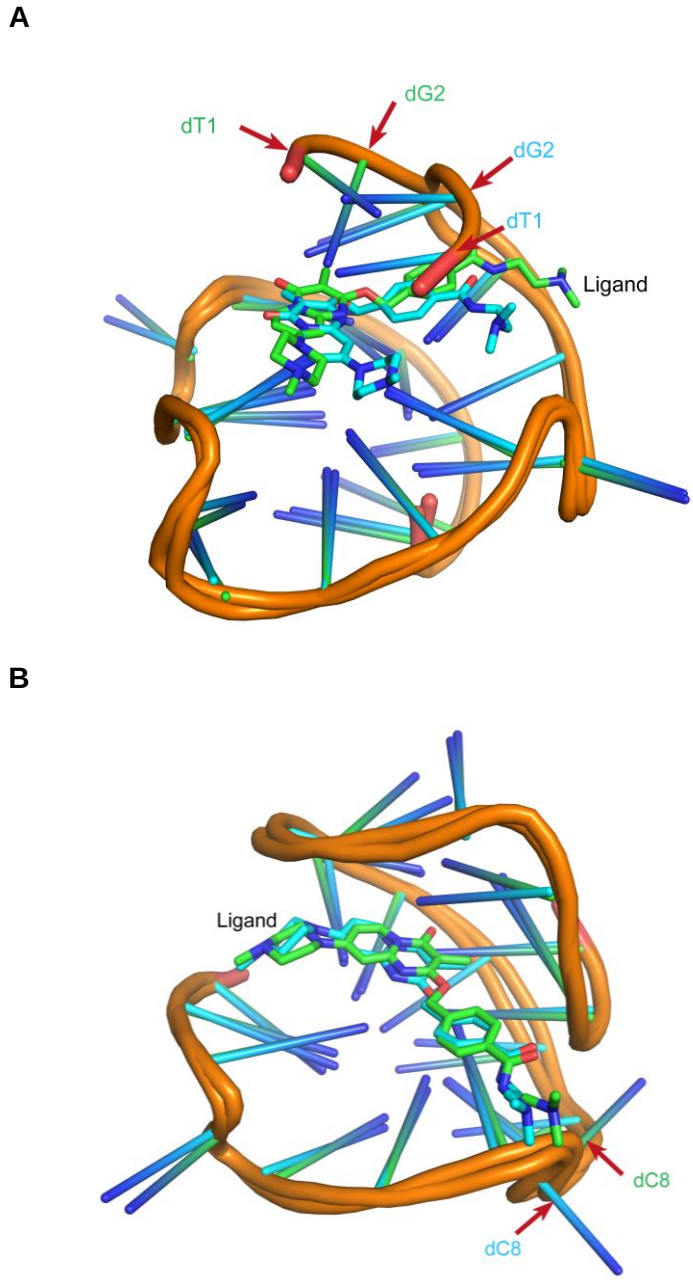

Figure S9. Comparison of representative structures of ensembles of c-*MYC* and c-*KIT1*-ligand **2** complexes. (A) Superposistion of representative structures of ensembles 1 and 2 of c-*MYC* complex. Major differences were observed in the orientations of dT1, dG2 and ligand; B) Superposition of representative structures of ensembles 1 and 2 of c-*KIT1*. Major differences were observed in the orientation of nucleotide dC8. Nucleotides are shown as ladders to avoid confusion. Green coloured ladders represent the ensemble 1 and cyan coloured ladders represent ensemble 2.

H-bonds between ligand 2 and *c-KIT*1 G4 DNA

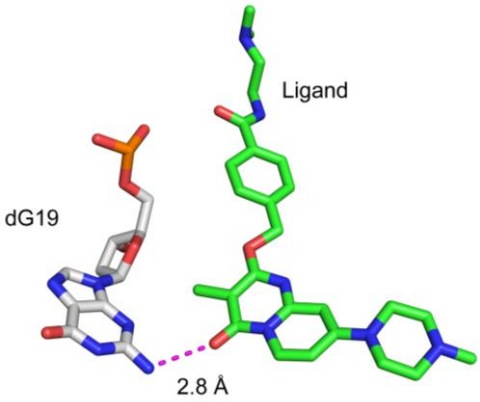

Figure S10. The H-bond that was observed between N-H of dG19 and O3 of ligand **2**. Cut off values of 3.5 Å and 135° are used for H-bond distance and angle respectively. The hydrogens on the ligand are removed for clarity and carbon atoms are represented using green, nitrogen atoms using blue, oxygen atoms using red and phosphorus using orange-red.

Reorientation of ligand during dynamics of c-*KIT1* complex

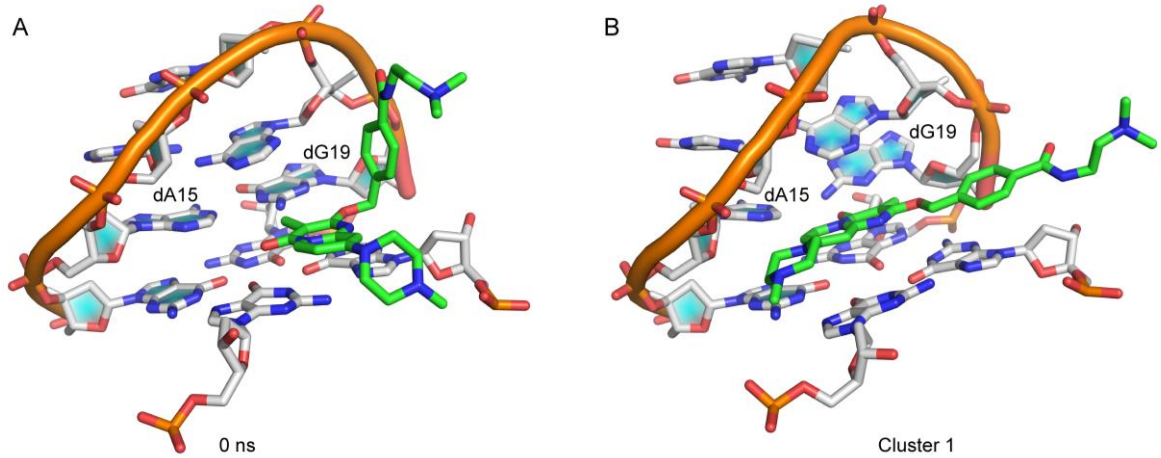

Figure S11. Comparison of c-*KIT1* complex structures before the start of dynamics and representative structure of the cluster from the dynamics. (A) Complex structure before the start of dynamics, ligand only partly stacks on the G-quartet; (B) Representative structure of major cluster, the ligand replaces the nucleotides dA15 and dG19 from the G-quartet and stacks completely on the G-quartet.

Reorientation of ligand 2 during dynamics of telomeric hybrid – 2 complex

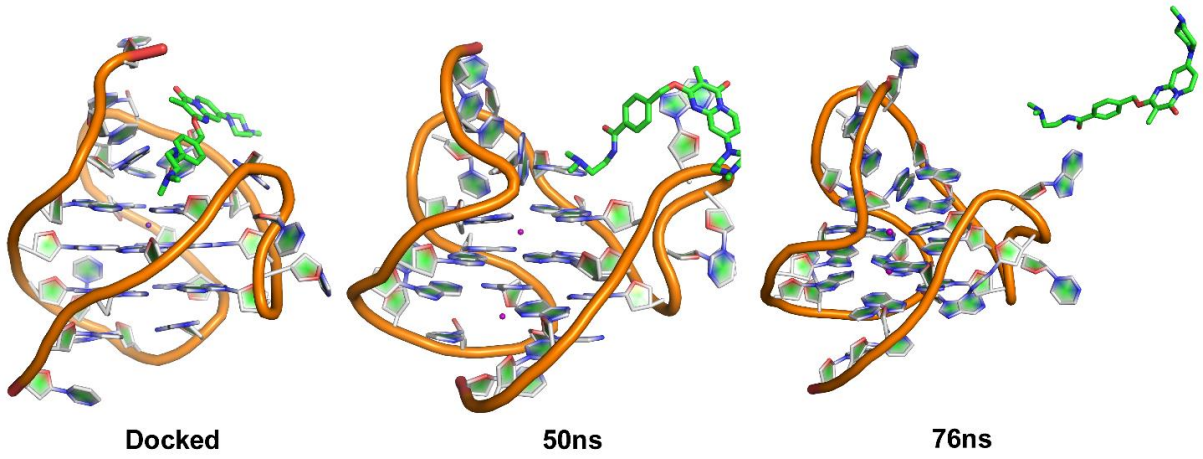

Figure S12. Binding of ligand 2 with telomeric hybrid -2 form G-quadruplex (PDB id: 2JPZ). Ligand **2** showed partial groove binding during docking but after 76ns of unrestrained dynamics, it lost binding with telomeric G-quadruplex. Oxygen atoms are shown using red and nitrogen atoms using blue. Carbon atoms are shown using green in ligand and using white in DNA. Potassium ions are shown using purple spheres

Oligonucleotides used for biophysical studies

Description	Sequence
Telomeric DNA	5'-AGGGTTAGGGTTAGGGTTAGGG-3'
c-MYC DNA	5'-TGAGGGTGGGTAGGGTGGGTAA-3'
c-KIT1 DNA	5'-GGGAGGGCGCTGGGAGGAGGG-3'
c-KIT2 DNA	5'-GGGCGGGCGCGAGGGAGGGG-3'
Duplex-17	5'-CCAGTTCGTAGTAACCC-3'
	5'-GGGTTACTA CGAACTGG-3'

Table S1. List of oligonucleotides used for the experiments.

Binding free energy components of the *c-MYC* and *c-KIT1* G4 DNA-ligand 2 complexes

	c-MYC **(PDB entry:2L7V)**	***c-KIT1*** **(PDB entry: 2O3M)**
ΔE_{ELEC}	−7.76 ± 8.11	− 5.54 ± 9.60
ΔE_{VDW}	− 66.48 ± 4.80	− 56.77 ± 4.04
$\Delta E_{MM}(\Delta E_{ELEC} + \Delta E_{VDW})$	− 74.25 ± 9.81	− 62.32 ± 11.26
ΔPB_{np}	− 4.68 ± 0.27	− 4.07 ± .0.23
ΔPB_{cal}	37.19 ± 7.76	30.26 ± 10.83
$\Delta PB_{solv}(\Delta PB_{np} + \Delta PB_{cal})$	32.50 ± 7.68	26.19 ± 9.93
$\Delta H_{PB}(\Delta E_{MM} + \Delta PB_{solv})$	**− 41.74 ± 4.52**	**− 36.12 ± 3.96**
ΔS_{TRANS}	− 13.16 ± 0.00	−13.16 ± 0.00
ΔS_{ROTA}	− 11.47 ± 0.03	−11.53 ± 0.02
ΔS_{VIBR}	5.47 ± 4.47	0.38 ± 4.33
$T\Delta S$	**− 19.16 ± 4.48**	**− 24.32 ± 4.33**
$\Delta G(\Delta H - T\Delta S)$	**− 22.57 ± 6.50**	**− 11.80 ± 5.80**

Table S2. Binding free energy components of *c-MYC* (left) and *c-KIT1* (right) G4 DNAs with the ligand **2** calculated from last 20 ns of 500 ns simulations. Every 5th frame and a total of 2000 frames have been considered for the calculations. The molecular-mechanical energy calculations were performed using MM/PBSA, and entropy calculations using nmode analysis. ΔE_{ELEC} is the electrostatic contribution. ΔE_{VDW} is the Vander Waals contribution. ΔE_{MM} is the total molecular-mechanical energy. ΔPB_{np} is the non-polar contribution to the solvation energy. ΔPB_{cal} is the electrostatic contribution to the solvation energy. ΔPB_{solv} is the total solvation energy. $T\Delta S$ is the solute entropic contribution, where ΔS is the sum of translational, rotational and vibrational entropies. $\Delta G(\Delta H - T\Delta S)$ is the estimated binding free energy. All the values are reported in kcal mol^{-1}. For nmode analysis parameters used were: drms = 0.05, dielec (distance dependent dielec) = 4, maxcyc = 20,000 and AMBER prescribed default values were used for PB calculations.

Experimental Section

General Methods. All reactions were conducted using oven-dried glassware under an atmosphere of argon (Ar) or nitrogen (N_2). Commercial grade reagents were used without further purification. Solvents were dried and distilled following standard literature protocols. Column chromatography was carried out using silica gel (100-200 mesh). TLC was performed on aluminium-backed plates coated with silica gel 60 with F_{254} indicator. The ^{1}H NMR (400 MHz) and ^{13}C NMR (100 MHz) were recorded using $CDCl_3$, DMSO-*d*$_6$ and CD_3OD on a Bruker instrument. ^{1}H NMR chemical shifts are expressed in parts per million (δ) relative to $CDCl_3$ (δ=7.26), [D_6]DMSO (δ=2.49) and CD_3OD (δ=3.31); ^{13}C NMR chemical shifts are expressed in parts per million (δ) relative to the $CDCl_3$ (δ=77.0), [D_6]DMSO (δ=39.7) and CD_3OD (δ=49.0). LCMS chromatograms and HPLC chromatograms were recorded on LCMS/MS API 2000 instrument with a DAD detector. High resolution mass spectra (HRMS) were obtained in positive ion electrospray ionization (ESI) mode using a Q-TOF analyzer.

Method A: General Procedure for Hydrolysis. To a stirred solution of ester, compound (1 equiv) in a mixture of THF, MeOH and H_2O (3:2:1, v/v) at room temperature was added LiOH (2.5 equiv). The reaction mixture was stirred for 16 h at the same temperature. The mixture was then concentrated under vacuum and the crude material was dissolved in H_2O. Aqueous layer was washed with ethyl acetate, acidified with 1N aqueous HCl (pH ~3) and the aqueous phase was concentrated to get crude hydrolyzed product.

Method B: General Procedure for Amide Coupling. To a stirred solution of crude hydrolyzed product (1 equiv) in DMF (6 mL/mmol) were added 1-(3-dimethylaminopropyl)-3-ethylcarbodiimide hydrochloride (2.5 equiv) and 1-hydroxybenzotriazole (1.5 equiv), and the mixture was stirred at room temperature for 10 min. Dimethylethane-1,2-diamine (2.5 equiv) and *N*,*N*-diisopropylethylamine (2.5 equiv) were added to it at room temperature and the resulting mixture was stirred for 16 h at the same temperature. The mixture was concentrated under vacuum and the crude material was purified by preparative HPLC to get the final amides.

Method C: General Procedure for Cyclization. A mixture of pyridine analogue (1 equiv) and diethyl methyl malonate (1 equiv) was heated at 140 °C for 24 h. The mixture was then cooled to room temperature, and the crude material was passed through silica gel column chromatography to give a semi-purified material, which was then taken into the next step

without further purification. This material thus obtained (1 equiv) was added to diphenyl ether (1.07 mL/mmol, pre-heated at 160 °C) under stirring. The reaction mixture was kept for 24 h at the same temperature. The mixture was cooled to room temperature and diluted with large volume of n-hexane while solid was precipitated. The solid was filtered, washed with hot n-hexane to give the cyclized product.

Method D: General Procedure for O-Benzylation. To a mixture of the cyclized product (1 equiv), potassium carbonate (3 equiv) in dry acetone (5 mL/mmol), 4-bromomethyl-benzoic acid methyl ester (1.5 equiv) was added. The reaction mixture was then heated at 65 °C for 3 h. The solvent was evaporated in vacuo; the crude residue was dissolved in ethyl acetate, and washed successively with water followed by brine. Ethyl acetate layer was separated, dried over Na_2SO_4, and evaporated in vacuum to get crude compound, which was purified by silica gel column chromatography to get pure alkylated product.

4-(3-Methyl-4-oxo-4H-pyrido[1,2-a]pyrimidin-2-yloxymethyl)-benzoic acid methyl ester (6a)

To a mixture of compound **5a**[1] (180 mg, 1.02 mmol), potassium carbonate (420 mg, 3.06 mmol) in dry acetone (10 mL) and 4-bromomethyl-benzoic acid methyl ester (350 mg, 1.53 mmol) were added. The reaction mixture was then heated at 65 °C for 3 h. The solvent was evaporated in vacuum; the crude residue was dissolved in ethyl acetate and washed successively with water followed by brine. Ethyl acetate layer was separated, dried over Na_2SO_4, and evaporated in vacuum to get crude compound, which was purified by silica gel column chromatography to get pure compound **6a** as light yellow solid (180 mg, 54.3%): R_f =0.3 (EtOAc/hexane 1:1); ^{1}H NMR (400 MHz, [D$_6$]DMSO): δ =2.07 (s, 3H), 3.85 (s, 3H), 5.60 (s, 2H), 7.30-7.34 (m, 1H), 7.56-7.63 (m, 3H), 7.92-7.99 (m, 3H), 8.95 ppm (d, J =7.0 Hz, 1H); ^{13}C NMR (100 MHz, $CDCl_3$): δ =8.7, 52.0, 67.1, 95.1, 114.3, 124.6, 127.0, 127.6, 129.4, 129.6, 135.6, 142.3, 147.9, 159.1, 164.4, 166.6 ppm; HRMS-ESI m/z $[M + H]^+$ calcd for $C_{18}H_{17}N_2O_4$: 325.1186, found: 325.1183.

***N*-(2-Dimethylamino-ethyl)-4-(3-methyl-4-oxo-4H-pyrido[1,2-a]pyrimidin-2-yloxymethyl)-benzamide (1)**

Method **A** was followed using compound **6a** (180 mg, crude, 0.55 mmol) in a mixture of THF, MeOH and H_2O (3:2:1, v/v) and LiOH (60 mg, 1.38 mmol) to get acid **8a** as a yellow

gummy liquid (200 mg, crude). This material was used in the next step without further purification. MS (ESI, 5.5 Kv) *m/z* (%) 311.0 (97.7) $[M+H]^+$. Method **B** was followed using crude compound **8a** (200 mg, 0.65 mmol) in DMF (4 mL), 1-(3-dimethylaminopropyl)-3-ethylcarbodiimide hydrochloride (308.1 mg, 1.62 mmol), 1-hydroxybenzotriazole (130.6 mg, 0.97 mmol), dimethylethane-1,2-diamine (0.11 mL, 0.97 mmol) and *N*,*N*-diisopropylethylamine (0.28 mL, 1.62 mmol) to get title compound **1** as light yellow solid (45 mg, 18%, over two steps): ^{1}H NMR (400 MHz, [D$_6$] DMSO): δ =2.05 (s, 3H), 2.16 (s, 6H), 2.36-2.40 (m, 2H), 3.33-3.34 (m, 2H), 5.55 (s, 2H), 7.32 (t, *J* =7.0 Hz, 1H), 7.54-7.60 (m, 3H), 7.83 (d, *J* = 8.0 Hz, 2H), 7.92-7.96 (m, 1H), 8.38 (m, 1H), 8.94 ppm (d, *J* =6.8 Hz, 1H); ^{13}C NMR (100 MHz, [D$_6$]DMSO): δ = 8.6, 37.3, 45.1, 58.0, 66.8, 92.8, 115.4, 124.3, 127.2, 133.9, 137.3, 140.0, 147.7, 158.1, 163.8, 165.7 ppm; HRMS-ESI *m/z* $[M+H]^+$ calcd for $C_{21}H_{24}N_4O_3$: 381.1916, found: 381.1916; HPLC analysis – Poroshell 120 EC-C18 (4.6 × 100 mm), Mobile phase: 0.05% TFA in H_2O: ACN, 200nm, t_R 5.56 min, 99.13%.

8-Chloro-2-hydroxy-3-methyl-pyrido[1,2-a]pyrimidin-4-one (5b)

Method **C** was followed using compound **4b** (2.0 g, 15.5 mmol) and diethyl methyl malonate (2.8 mL, 15.5 mmol) to give a crude material, which was taken into the following step without further purification. MS (ESI, 5.5 Kv) *m/z* (%) 256.6 (95.3) $[M+H]^+$. To the crude material thus obtained (1.2 g, 4.68 mmol) was added to diphenyl ether (5 mL, pre-heated at 160 °C) by following the method **C** to give the compound **5b** as off white solid (500 mg, 51%, over two steps): ^{1}H NMR (400 MHz, [D$_6$]DMSO) δ =1.90 (s, 3H), 7.32 (dd, *J* =2.0, 2.1 Hz, 1H), 7.46 (d, *J* =2.0 Hz, 1H), 8.86 (d, *J* =7.5 Hz, 1H), 12.02 ppm (s, 1H); ^{13}C NMR (100 MHz, D_2O + NaOD) δ =8.8, 95.8, 113.0, 118.7, 126.6, 141.0, 147.3, 157.2, 171.9 ppm; HRMS-ESI *m/z* $[M+H]^+$ calcd for $C_9H_8ClN_2O_2$: 211.0195, found: 211.0269.

4-(8-Chloro-3-methyl-4-oxo-4H-pyrido[1,2-a]pyrimidin-2-yloxymethyl)-benzoic acid methyl ester (6b)

Method **D** was followed using a mixture of the compound **5b** (500 mg, 2.38 mmol), potassium carbonate (990 mg, 7.14 mmol) in dry acetone (12 mL), and 4-bromomethyl-benzoic acid methyl ester (820 mg, 3.57 mmol) to get pure compound **6b** as light yellow solid (600 mg, 70%): R_f =0.4 (EtOAc/hexane 1:3); ^{1}H NMR (400 MHz, [D$_6$]DMSO) δ =2.04 (s, 3H), 3.84 (s, 3H), 5.58 (s, 2H), 7.36 (dd, *J* =2.2, 2.24 Hz, 1H), 7.61 (d, *J* =8.2 Hz, 2H), 7.74 (d, *J* =2.1 Hz, 1H), 7.97 (d, *J* =8.2 Hz, 2H), 8.89 ppm (d, *J* =7.5 Hz, 1H); ^{13}C NMR (100

MHz, $CDCl_3$): δ =8.7, 52.0, 67.4, 95.5, 116.0, 123.0, 127.0, 128.6, 129.5, 129.7, 142.1, 142.9, 147.7, 158.7, 164.7, 166.7 ppm; HRMS-ESI *m/z* $[M+H]^+$ calcd for $C_{18}H_{16}ClN_2O_4$: 359.0794, found: 359.0793.

4-[3-Methyl-8-(4-methyl-piperazin-1-yl)-4-oxo-4H-pyrido[1,2-a]pyrimidin-2-yloxymethyl]-benzoic acid methyl ester (7b)

To a solution of compound **6b** (200 mg, 0.558 mmol) in DMSO (4 mL) was added dipotassium hydrogenphosphate (390 mg, 2.23 mmol) and 1-methyl-piperazine (0.093 mL, 0.837 mmol) at room temperature and the reaction mixture was then stirred at 110 °C for 1.5 h. The mixture was cooled to room temperature and diluted with water. Organic layer was extracted with DCM, washed with brine, dried over Na_2SO_4, concentrated under vacuum. The crude material was purified by column chromatography to get pure compound **7b** as off white solid (140 mg, 60%): R_f =0.2 (DCM/MeOH 9.5:0.5); ^{1}H NMR (400 MHz, [D_6]DMSO): δ =1.96 (s, 3H), 2.22 (s, 3H), 2.42 (m, 4H), 3.50-3.51 (m, 4H), 3.85 (s, 3H), 5.53 (s, 2H), 6.54 (d, *J* =2.6 Hz, 1H), 7.15-7.18 (m, 1H), 7.58 (d, *J* =8.2 Hz, 2H), 7.97 (d, *J* =8.2 Hz, 2H), 8.64 ppm (d, *J* =8.1 Hz, 1H); ^{13}C NMR (100 MHz, CD_3OD + 2 drops $CDCl_3$): δ =45.0, 45.8, 51.6, 54.1, 66.9, 90.1, 99.8, 106.2, 127.1, 127.9, 129.6, 143.2, 150.1, 154.4, 159.7, 165.9, 167.3 ppm; MS (ESI, 5.5 Kv) *m/z* (%) 422.8 (98.5) $[M+H]^+$.

***N*-(2-Dimethylamino-ethyl)-4-[3-methyl-8-(4-methyl-piperazin-1-yl)-4-oxo-4H-pyrido[1,2-a]pyrimidin-2-yloxy methyl]-benzamide (2)**

Method **A** was followed using compound **7b** (120 mg, 0.284 mmol) in a mixture of THF, MeOH and H_2O (3:2:1, v/v) and LiOH (36 mg, 0.853 mmol) to get the compound **8b** as a yellow gummy liquid (150 mg, crude). This material was used in the next step without further purification. MS (ESI, 5.5 Kv) *m/z* (%) 409.0 (94.7) $[M+H]^+$. Method **B** was followed using crude compound **8b** (140 mg, 0.34 mmol) in DMF (3 mL), 1-(3-dimethylaminopropyl)-3-ethylcarbodiimide hydrochloride (163.2 mg, 0.85 mmol) , 1-hydroxybenzotriazole (68.8 mg, 0.51 mmol), dimethyl-ethane-1,2-diamine (0.055 mL, 0.51 mmol) and *N*,*N*-diisopropylethylamine (0.148 mL, 0.85 mmol) to get the titled compound **2** as off white solid (26 mg, 16%, over two steps): ^{1}H NMR (400 MHz, CD_3OD): δ =2.05 (s, 3H), 2.33-2.34 (s, 9H), 2.56-2.61 (m, 6H), 3.50-3.58 (m, 6H), 5.53 (s, 2H), 6.65 (d, *J* =2.7 Hz, 1H), 7.08-7.10 (m, 1H), 7.52 (d, *J* =8.2 Hz, 2H), 7.83 (d, *J* =8.2 Hz, 2H), 8.73 ppm (d, *J* =8.1 Hz, 1H); ^{13}C NMR (100 MHz, CD_3OD): δ =7.6, 37.4, 44.4, 45.0, 45.9, 54.3, 58.2, 67.1, 89.9, 99.7, 106.3,

127.5, 128.0, 133.8, 141.8, 150.3, 154.6, 159.8, 166.1, 168.9 ppm; HRMS-ESI *m/z* $[M+H]^+$ calcd for $C_{26}H_{34}N_6O_3$: 479.2759, found: 479.2759; HPLC analysis – Poroshell 120 EC-C18 (4.6 × 100 mm), Mobile phase: 0.05% TFA in H_2O: ACN, 230nm, t_R 4.59 min, 99.39%.

7,8-Dichloro-2-hydroxy-3-methyl-pyrido[1,2-a]pyrimidin-4-one (5c)

To a stirred solution of compound **4b** (1.29 g, 10.07 mmol) in ethyl acetate (50 mL) was added *N*-chlorosuccinimide (2.01 g, 15.11 mmol) and the mixture was stirred at room temperature for 24 h. Solids were precipitated and the supernatant liquid was decanted and transferred to a separatory funnel. This layer is washed with saturated aqueous sodium bisulfite solution followed by brine, dried over $MgSO_4$ and concentrated under vacuum to get crude solid **4c**, which was used in the next step without further purification. MS (ESI, 5.5 Kv) *m/z* (%) 163.0 (95.6) $[M+H]^+$. Method **C** was followed using a mixture of crude compound **4c** (2.4 g) and diethyl methyl malonate (6.4 mL, 37.03 mmol) to give a solid (1.4 g, crude) which was taken into the following step without further purification. The crude material thus obtained (1.4 g) and diphenyl ether (8 mL, pre-heated at 160 °C) were treated to give the compound **5c** as off white solid (400 mg, 34%, over three steps): ^{1}H NMR (400 MHz, [D_6]DMSO): δ =1.92 (s, 3H), 6.67 (s, 1H), 7.71 (s, 1H), 8.04 (s, 1H), 8.98 ppm (s, 1H); ^{13}C NMR (100 MHz, [D_6]DMSO): δ =9.0, 91.6, 120.2, 121.8, 127.1, 141.2, 145.9, 156.4, 164.2 ppm; HRMS-ESI *m/z* $[M+H]^+$ calcd for $C_9H_7Cl_2N_2O_2$: 244.9871, found: 244.9879.

4-(7,8-Dichloro-3-methyl-4-oxo-4H-pyrido[1,2-a]pyrimidin-2-yloxymethyl)-benzoic acid methyl ester (6c)

Method **D** was followed using a mixture of the compound **5c** (240 mg, 0.983 mmol), potassium carbonate (406 mg, 2.94 mmol) in dry acetone (10 mL), and 4-bromomethyl-benzoic acid methyl ester (338 mg, 1.47 mmol) to get the compound **6c** as light yellow solid (250 mg, 65%): R_f =0.4 (EtOAc/hexane 1:1.6); ^{1}H NMR (400 MHz, [D_6]DMSO): δ =2.05 (s, 3H), 3.85 (s, 3H), 5.58 (s, 2H), 7.61 (d, *J* =7.9 Hz, 2H), 7.96-8.00 (m, 3H), 9.03 ppm (s, 1H); ^{13}C NMR (100 MHz, $CDCl_3$): δ =8.9, 52.1, 67.6, 96.1, 122.5, 124.4, 126.9, 127.1, 129.7, 129.8, 141.9, 142.1, 146.2, 157.8, 164.7, 166.7 ppm; HRMS-ESI *m/z* $[M+H]^+$ calcd for $C_{18}H_{15}Cl_2N_2O_4$: 393.0407, found: 393.0403.

4-[7-Chloro-3-methyl-8-(4-methyl-piperazin-1-yl)-4-oxo-4H-pyrido[1,2-a]pyrimidin-2-yloxymethyl]-benzoic acid methyl ester (7c)

To a solution of the compound **6c** (250 mg, 0.637 mmol) in DMSO (5 mL) was added dipotassium hydrogenphosphate (440 mg, 2.55 mmol) and 1-methyl-piperazine (0.106 mL, 0.955 mmol) at room temperature and the reaction mixture was then stirred at 110 °C for 1.5 h. The mixture was cooled to room temperature and diluted with water. Organic layer was extracted with DCM, washed with brine, dried over Na_2SO_4, concentrated under vacuo. The crude material was purified by column chromatography to get pure compound **7c** as off white solid (280 mg, 96%): R_f =0.3 (DCM/MeOH 9.5:0.5); ^{1}H NMR (400 MHz, CD_3OD): δ =2.09 (s, 3H), 2.37 (s, 3H), 2.66 (m, 4H), 3.36 (m, 4H), 3.89 (s, 3H), 5.57 (s, 2H), 6.92 (s, 1H), 7.54 (d, J =8.2 Hz, 2H), 8.01 (d, J =8.2 Hz, 2H), 8.89 ppm (s, 1H); ^{13}C NMR (100 MHz, [D_6]DMSO): δ =8.5, 28.9, 45.4, 49.5, 52.0, 53.9, 66.4, 90.3, 108.8, 118.4, 126.9, 127.1, 128.7, 129.2, 142.6, 147.8, 154.9, 157.1, 164.3, 165.8 ppm; HRMS-ESI *m/z* $[M+H]^+$ calcd for $C_{23}H_{26}ClN_4O_4$: 457.1632, found: 457.1637.

4-[7-Chloro-3-methyl-8-(4-methyl-piperazin-1-yl)-4-oxo-4H-pyrido[1,2-a]pyrimidin-2-yloxymethyl]-N-(2-dimethylamino-ethyl)-benzamide (3)

Method **A** was followed using compound **7c** (270 mg, 0.592 mmol) in a mixture of THF, MeOH and H_2O (3:2:1, v/v) and LiOH (74.5 mg, 1.77 mmol) to get acid compound **8c** as a white gummy solid (360 mg, crude) which was used in the next step without further purification. MS (ESI, 5.5 Kv) *m/z* (%) 443.0 (78.4) $[M+H]^+$. Method **B** was followed using crude compound **8c** (360 mg) in DMF (4 mL), 1-(3-dimethylaminopropyl)-3-ethylcarbodiimide hydrochloride (388.9 mg, 2.02 mmol), 1-hydroxybenzotriazole (164.9 mg, 1.21 mmol), Dimethyl-ethane-1,2-diamine (0.132 mL, 1.22 mmol) and *N*,*N*-diisopropylethylamine (0.355 mL, 2.02 mmol) to get title compound **3** as off white solid (30 mg, 9.8%, over two steps): ^{1}H NMR (400 MHz, CD_3OD): δ =2.08 (s, 3H), 2.37 (m, 6H), 2.60-2.66 (m, 6H), 3.37 (m, 4H), 3.51-3.54 (m, 2H), 5.57 (s, 2H), 6.94 (s, 1H), 7.54 (d, J =8.1 Hz, 2H), 7.84 (d, J =8.1 Hz, 2H), 8.91 ppm (s, 1H); ^{13}C NMR (100 MHz, [D_6]DMSO): δ =8.5, 36.9, 44.8, 45.4, 49.5, 53.9, 57.8, 66.6, 90.3, 108.8, 118.3, 126.9, 127.2, 133.7, 140.1, 147.8, 154.9, 157.1, 164.3, 165.8 ppm; HRMS-ESI *m/z* $[M+H]^+$ calcd for $C_{26}H_{33}ClN_6O_3$: 513.2379, found: 513.2379; HPLC analysis - Poroshell 120 EC-C18 (4.6x100 mm), Mobile phase: 0.05% TFA in H2O: ACN, 240nm, t_R 4.92 min, 99.89%.

DNA Oligonucleotides and ligand stock solutions

The oligonucleotides utilized for the biophysical studies (Table S1) were synthesized on a Mermade 4 DNA synthesizer and purified by PAGE (20%, 7M urea). The ligands **2** sock solution (5 mM) was prepared in water, and ligands **1** and **3** stock solutions (5 mM) were prepared in 50% DMSO-water (v/v). The stocks were further diluted using water, and used in the experiments.

CD Titration Studies

CD spectra were recorded on a Jasco J-815 CD spectrophotometer using a quartz cuvette having 1.0 mm path length in the wavelength range of 220-320 nm. The scanning speed of the instrument was set to100 nm/min and the response time was 2 sec. The DNA strand concentration used was 12.5 µM and the baseline was measured using 50 mM Tris buffer, pH 7.2. Each spectrum is an average of 3 measurements at 25 °C. All the spectra were analysed using Origin 8.0 software.

CD Melting Studies

For the CD melting studies, 10 µM DNA strand concentration in 10 mM lithium or sodium cacodylate buffer, pH 7.2, required amount of monovalent salts (LiCl and KCl or NaCl) and 5 molar equivalents of ligands (50 µM for G4 DNAs and 75 µM for duplex DNA) were used. Telomeric DNA (in 10 mM NaCl, 90 mM LiCl and 10 mM sodium cacodylate buffer, pH 7.2 for Na^+ conditions and in 10 mM KCl, 90 mM LiCl and 10 mM lithium cacodylate buffer, pH 7.2 for K^+ conditions), *c-MYC* DNA (in 1mM KCl, 99 mM LiCl and 10 mM lithium cacodylate buffer , pH 7.2), *c-KIT1* DNA (in 10 mM KCl, 90 mM LiCl and lithium cacodylate buffer , pH 7.2), and *c-KIT2* DNA (in 1 mM KCl, 99 mM LiCl and lithium cacodylate buffer , pH 7.2) were annealed by heating at 95 °C for 5 min followed by gradual cooling to room temperature. Ligands (5 equivalents) were added to the annealed DNAs (250 µl) and were kept at 4 °C overnight. Thermal melting was monitored at 295 nm and 263 nm for telomeric and promoter G4 DNAs respectively at the heating rate of 1 °C/min. $T_{1/2}$ values were determined from sigmoidal curve fit using Boltzmann function in Origin 8.0 software.

UV Melting Studies

UV melting studies were carried out on a Varian Cary UV 100 Bio spectrometer using a quartz cuvette having 10 mm path length. The strand concentration of duplex DNA was 5 µM

and that of the ligand was 25 μM. The DNA (5 μM) in 10 mM KCl, 90 mM LiCl and 10 mM lithium cacodylate buffer, pH 7.2 was annealed by heating at 95 °C for 5 min followed by gradual cooling to room temperature. Ligands were added to the annealed DNAs and were kept at 4 °C for overnight after making the final volume as 500 μL. Thermal melting was monitored at 260 nm in the range of 20-95 °C at the heating rate of 1 °C/min. $T_{1/2}$ values were determined from sigmoidal curve fit using Boltzmann function in Origin 8.0 software.

Isothermal Titration Calorimetry

Calorimetric experiments were carried out using a MicroCal iTC-200. All the DNA samples (25 μM in 100 mM KCl and 10 mM Lithium cacodylate buffer, pH 7.2) were pre-annealed by heating at 95 °C for 5 minutes, and then gradual cooling to room temperature over 3-4 h. Titrations were carried out by overfilling the DNA samples (25 μM) in the sample cell (~300 μL) and by titrating with ligand solution (1 mM under similar salt and buffer conditions) over 40 injections. During the experiment, temperature of the sample and reference cells was maintained at 25 °C. Volume for each ligand injection was 1 μL for 2 s, and time interval between successive injections was 120 s. To nullify the heats of dilution, same concentration of ligand was titrated against the buffer under similar conditions, and was subtracted from the raw data prior to the curve fitting. The dilution corrected data were fitted using a sequential binding model in Origin 7 to derive the thermodynamic parameters for the DNA-ligand interactions.

Molecular Modeling and Dynamics Studies

The structure of ligand **2** was energy optimized in Gaussian 09[2] at a theoretical level 6-31+G**. Conformational effects were taken into account while optimizing the ligand **2** (Figure S6). The optimized ligand **2** was then docked with c-*MYC* (PDB ID: 2L7V)[3] and c-*KIT1* (PDB ID: 2O3M)[4] structures using AutoDock4. Lamarckian genetic algorithm was used for docking to generate 250 independent conformations. The 5'-end nucleotide dA of c-*KIT1* was removed from PDB structure in order to facilitate the docking. Based on docking results, restrained electrostatic potential charges were calculated using Gaussian 09[2] and fitted using antechamber of AMBER 14.[5] xLeap was used to prepare the systems for simulations. Generalized AMBER force filed (GAFF)[6] and AMBER *FF* (ff14SB) were used for ligand **2** and DNA respectively. The systems were neutralized by adding K^+ ions. Solvation was carried out using TIP3P water molecules extending up to 10 Å in a rectangular

box. These complexes were then subjected to 10000 steps of minimization, 100 ps of heating, 100 ps of density equilibration followed by 800 ps of equilibration. Later, the systems were subjected to 500 ns of unrestrained dynamics using GPU accelerated version of PMEMD of AMBER14.[5] The coordinates were saved for every 2 ps in all the MD processes. Binding free energies were estimated using MM-PBSA[7] method over last 20 ns. Every 5th frame (every 10 ps) and a total of 2000 frames were used for binding energy calculations. The trajectory analysis was carried out using CPPTRAJ[8] and UCSF Chimera[9]. RMSD values of heavy atoms, per nucleotide-RMSF values, H-bonds and Hoogsteen H-bond occupancies were all calculated for every 5th frame (every 10 ps) and a total of 50 000 frames were used. Cutoff values 3.5 Å and 135° were used for defining H-bonds. UCSF Chimera was used for visualization of MD trajectories. Pictures were rendered using PyMol(www.pymol.org).

^{1}H NMR spectrum of compound 6a

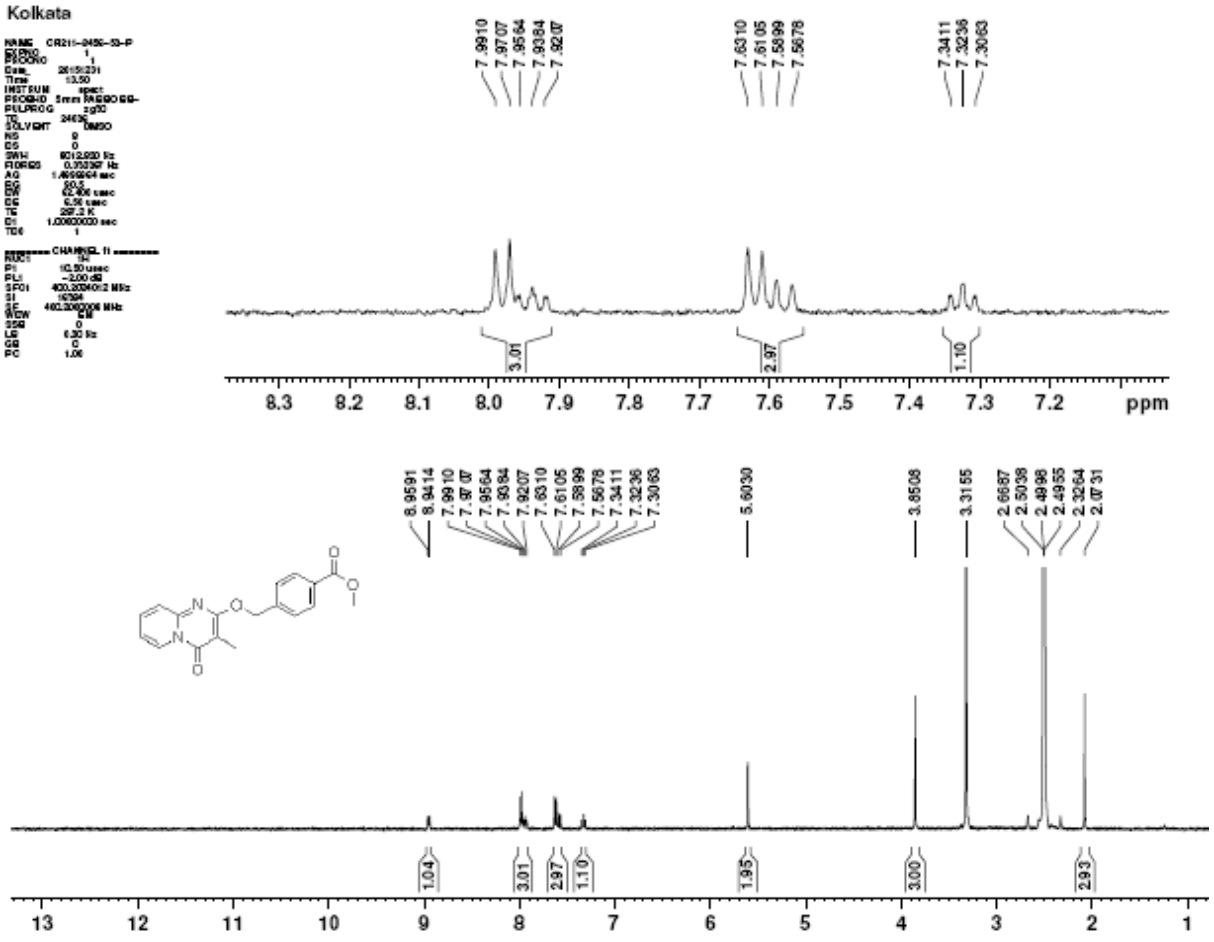

^{13}C NMR spectrum of compound 6a

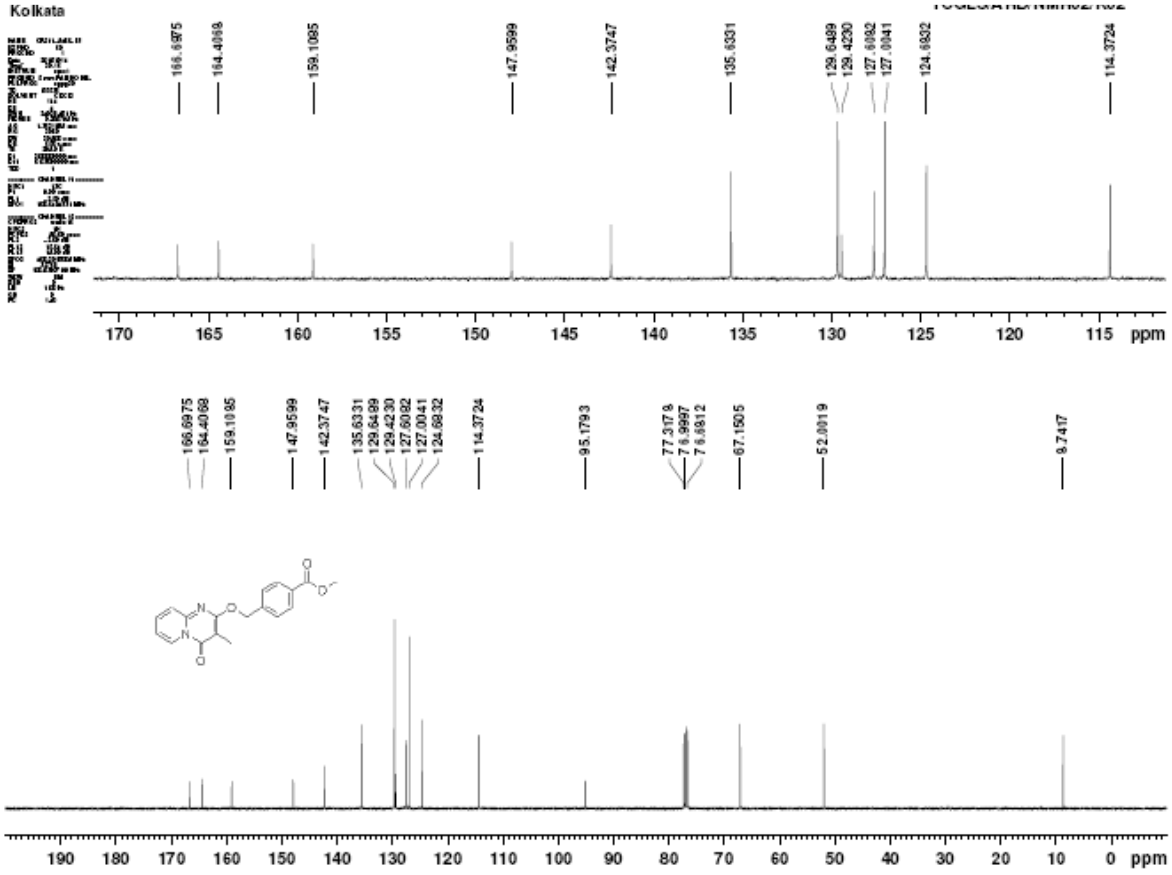

^{1}H NMR spectrum of compound 1

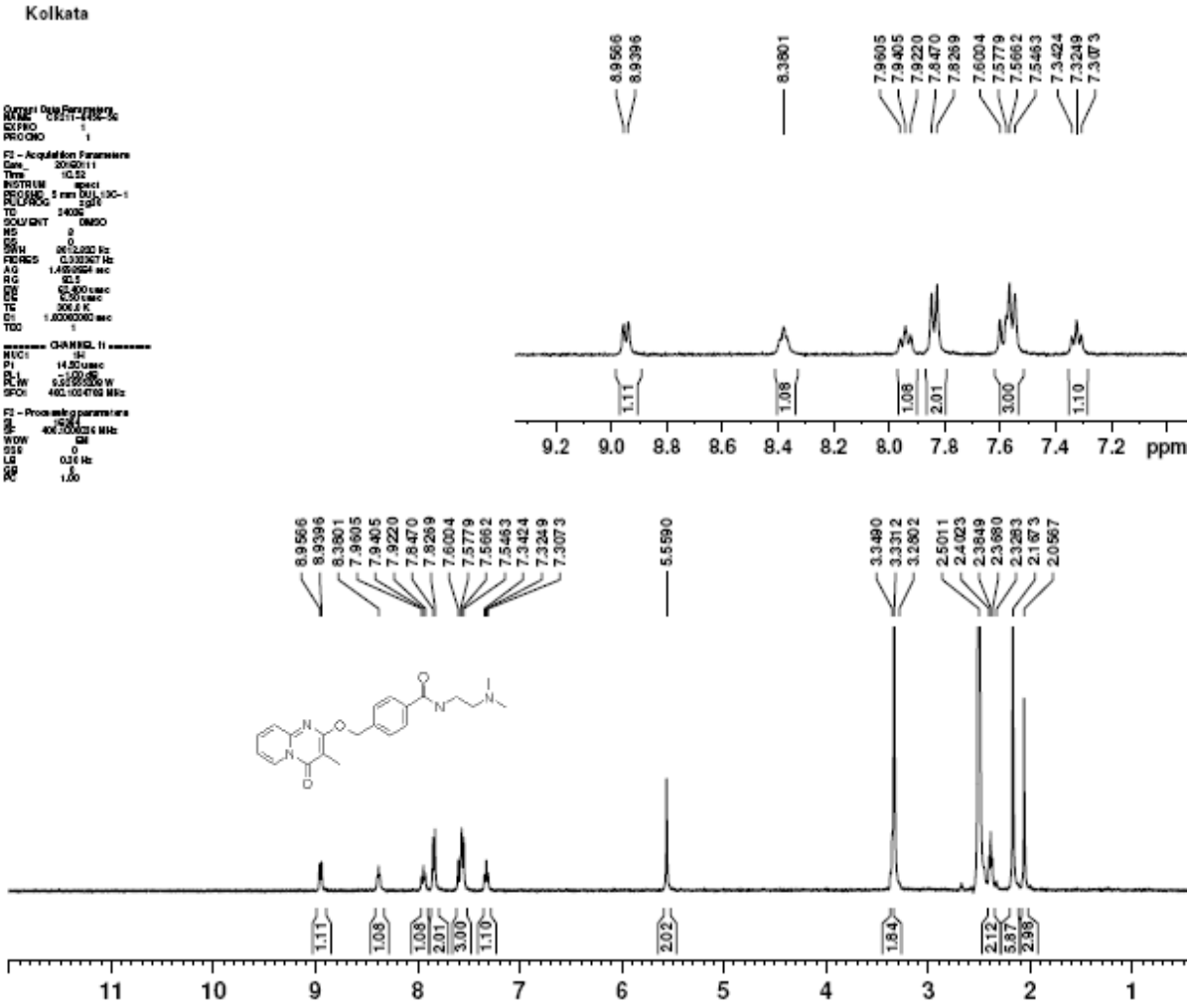

^{13}C NMR spectrum of compound 1

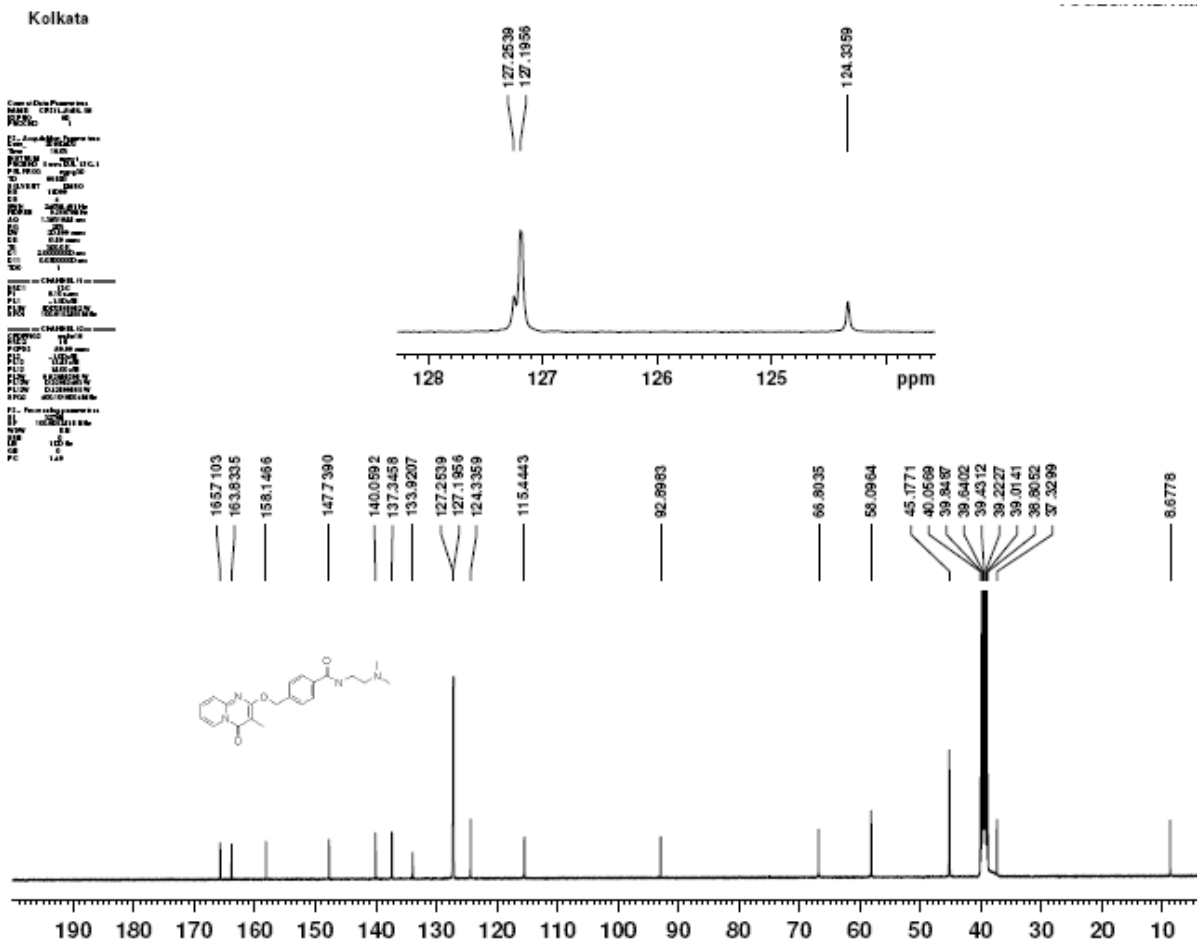

APT spectrum of compound 1

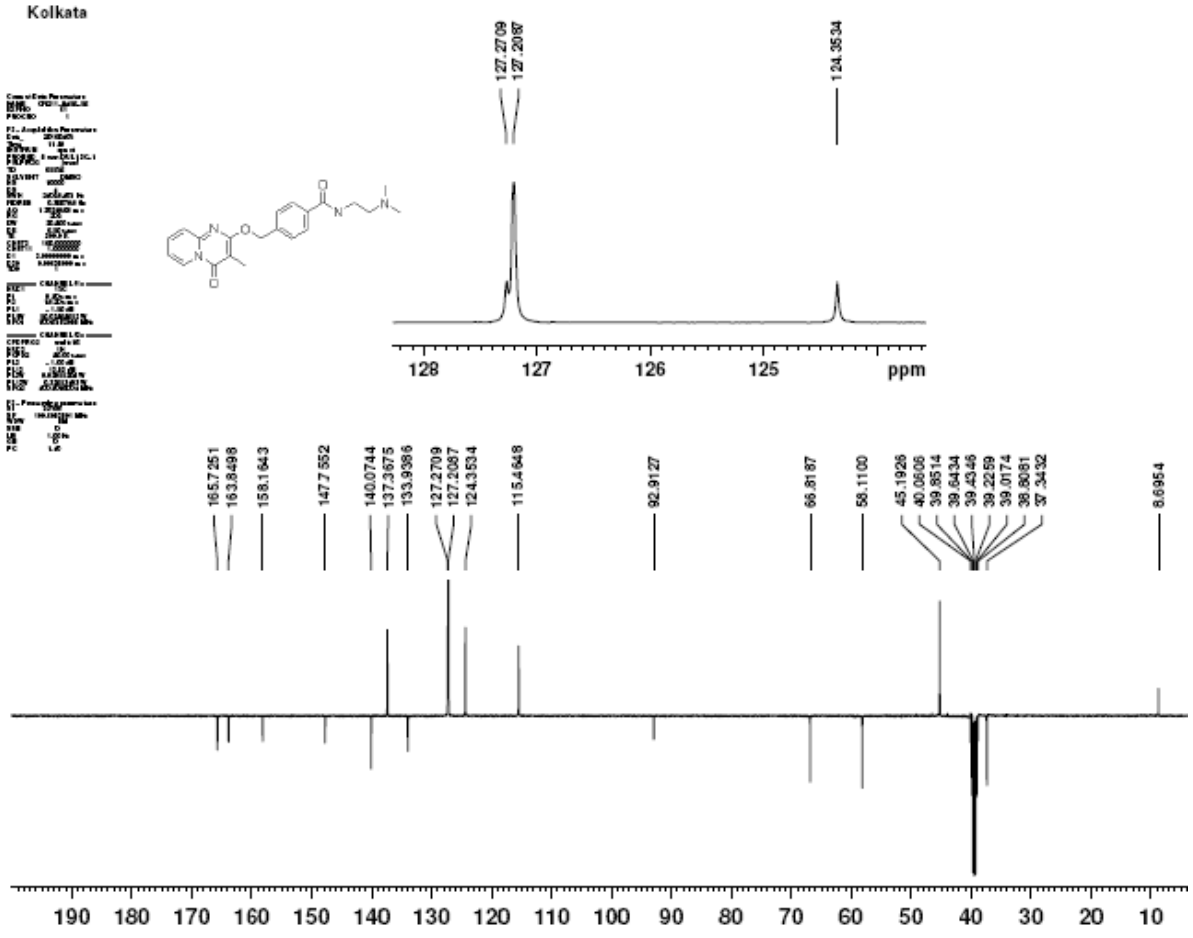

HPLC chromatogram of compound 1

```
Sample Name:CR211-8456-56
Column ID:Poroshell  120 EC-C18 (4.6*100mm).2.7um; Dilu
ent: MeOH
B: ACN A : 0.05% TFA IN WATER                                              ->
Injection Date  : Fri, 29. Jan. 2016 11:32:33   Location   :    Vial 92
Sample Name     : CR211-8456-56                       Inj. No.->        1
Acq Operator    : PRIYA                         Inj. Vol.  :       2 µl

Analysis Method : C:\CHEM32\1\METHODS\GEN_J2.M
Last Changed    : Fri, 29. Jan. 2016, 11:52:17 am
                  (modified after loading)

Acq. Method     : C:\CHEM32\1\DATA\2015\JAN-16\290116C 2016-01-29 09-04-
                  28\GEN_J.M

                                                  Ref :PC/  29.01.16/1128
```

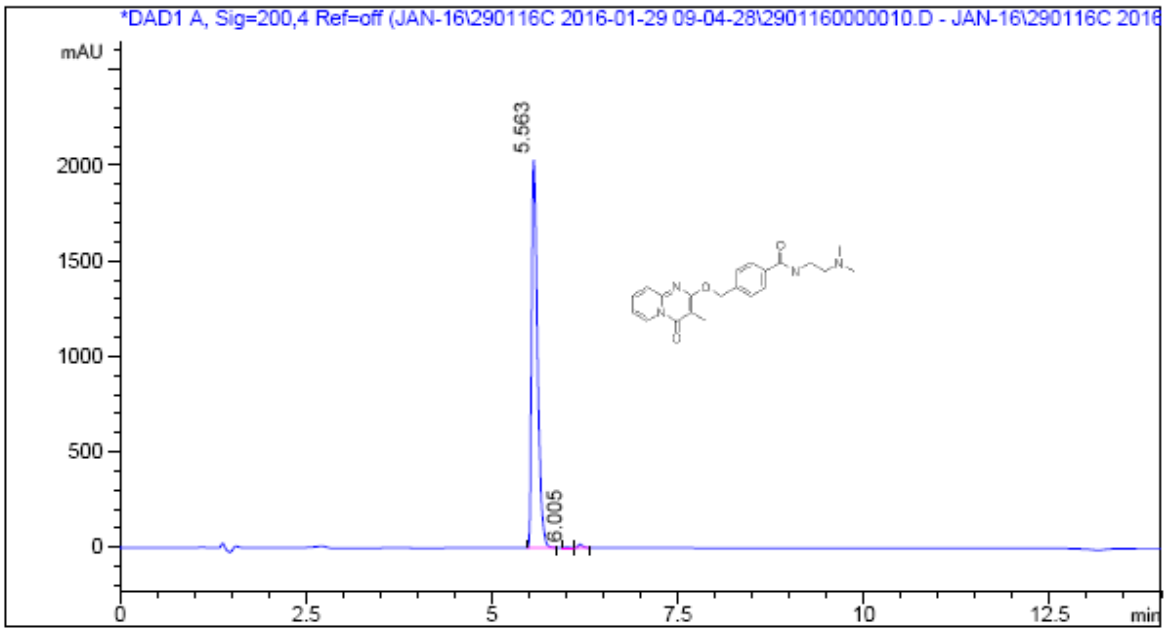


```
================================================================================

================================================================================
Signal  1 :DAD1 A, Sig=200,4 Ref=off

|Peak|   RT    |   Area    | Area % |
| #  |  [min]  |           |        |
|----|---------|-----------|--------|
|   1|     5.56|  11128.72|   99.13|
|   2|     6.01|     21.48|    0.19|
|   3|     6.19|     76.01|    0.68|
-----------------------------------
================================================================================
                          *** End of Report ***
```

^{1}H NMR spectrum of compound 5b

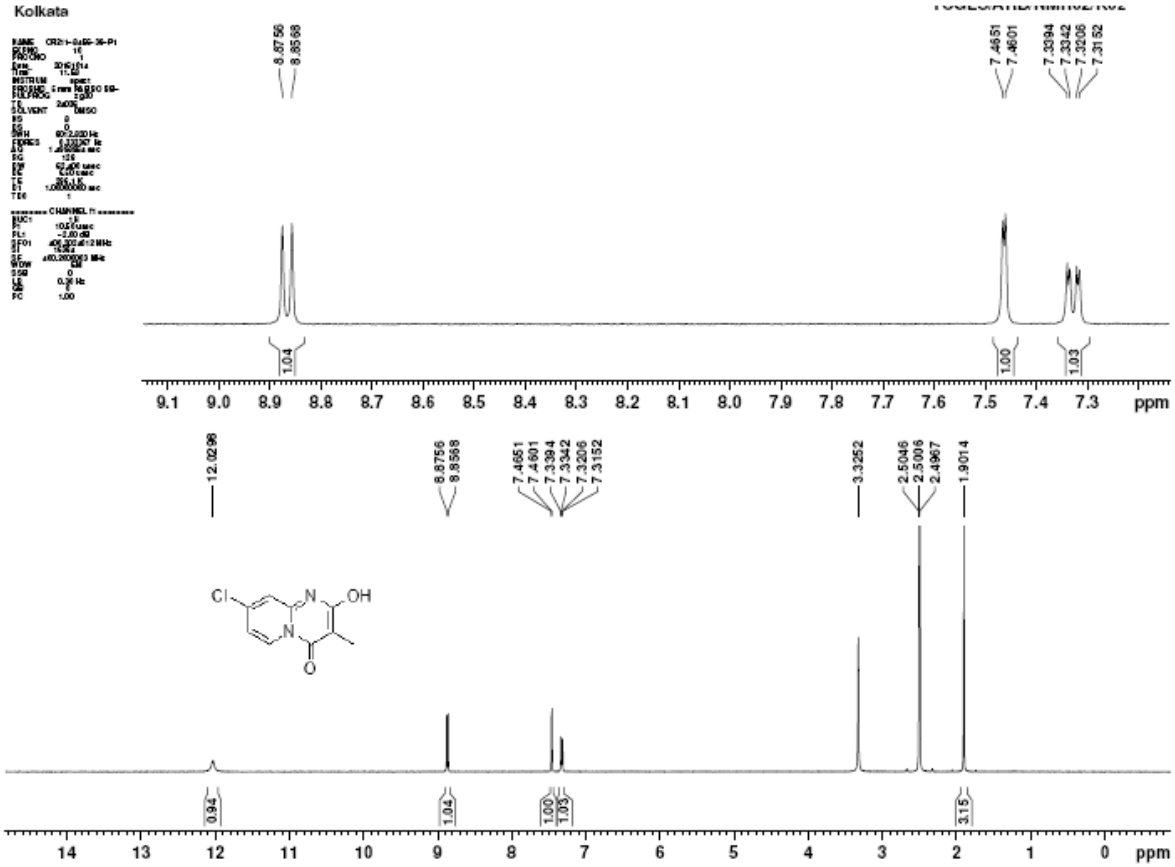

^{13}C NMR spectrum of compound 5b

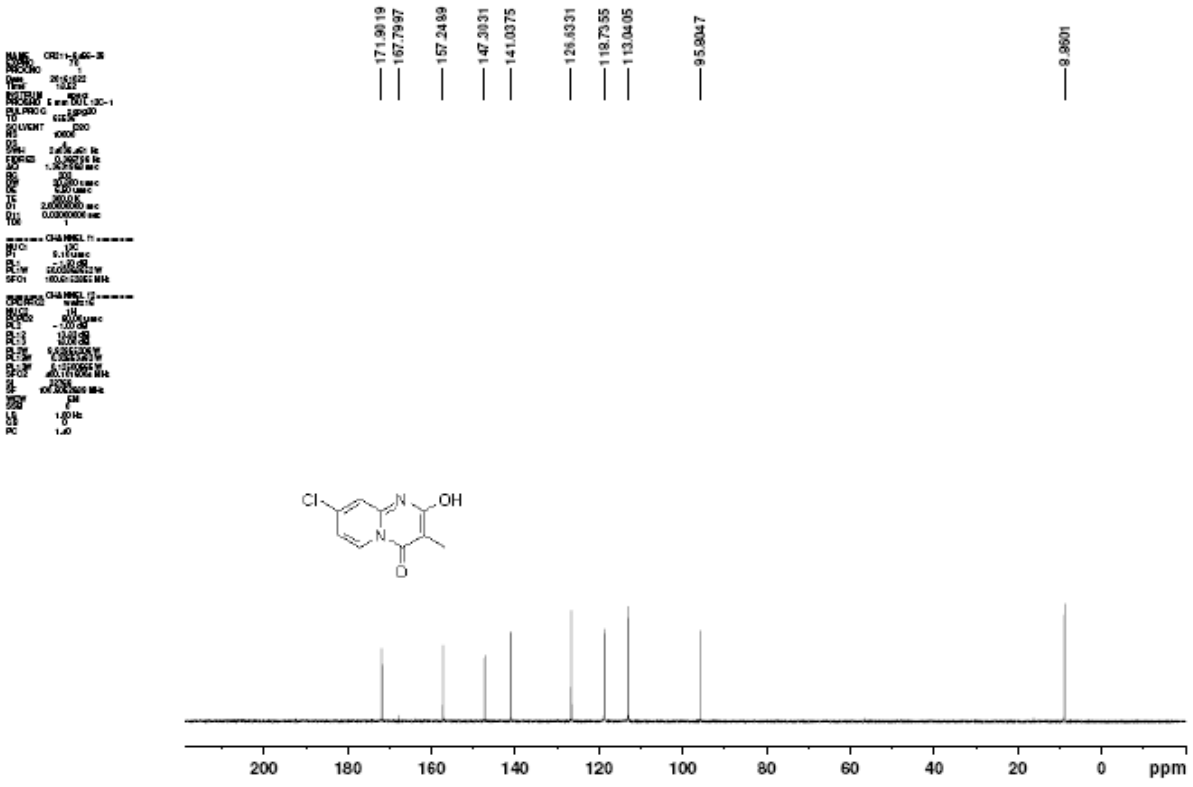

APT spectrum of compound 5b

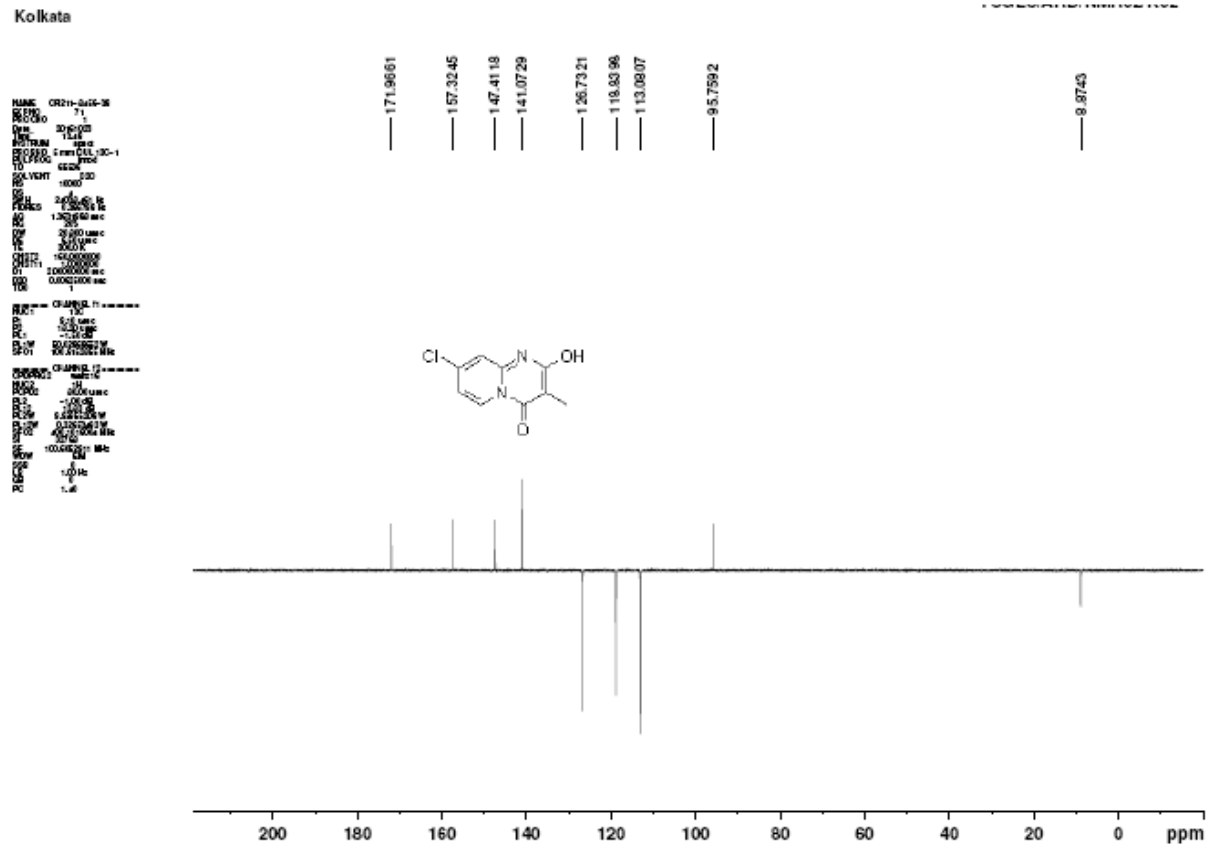

^{1}H NMR spectrum of compound 6b

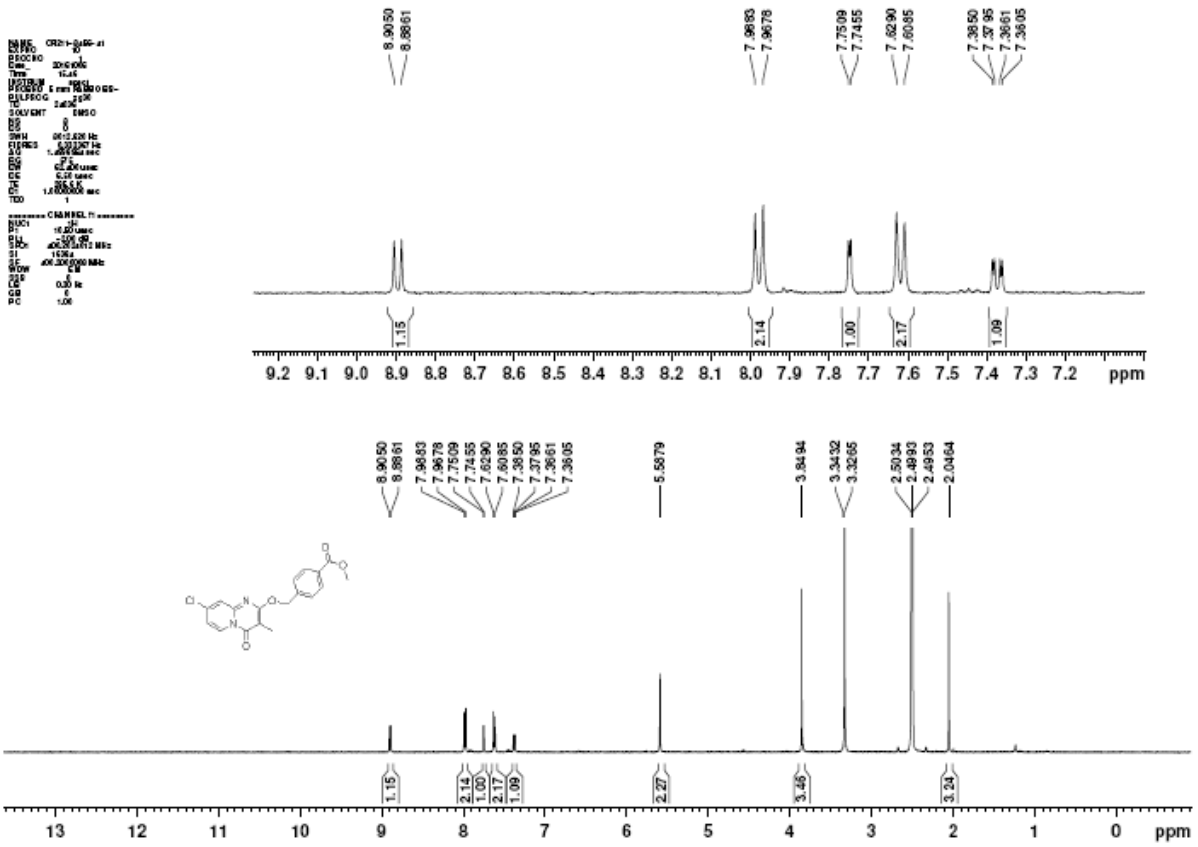

^{13}C NMR spectrum of compound 6b

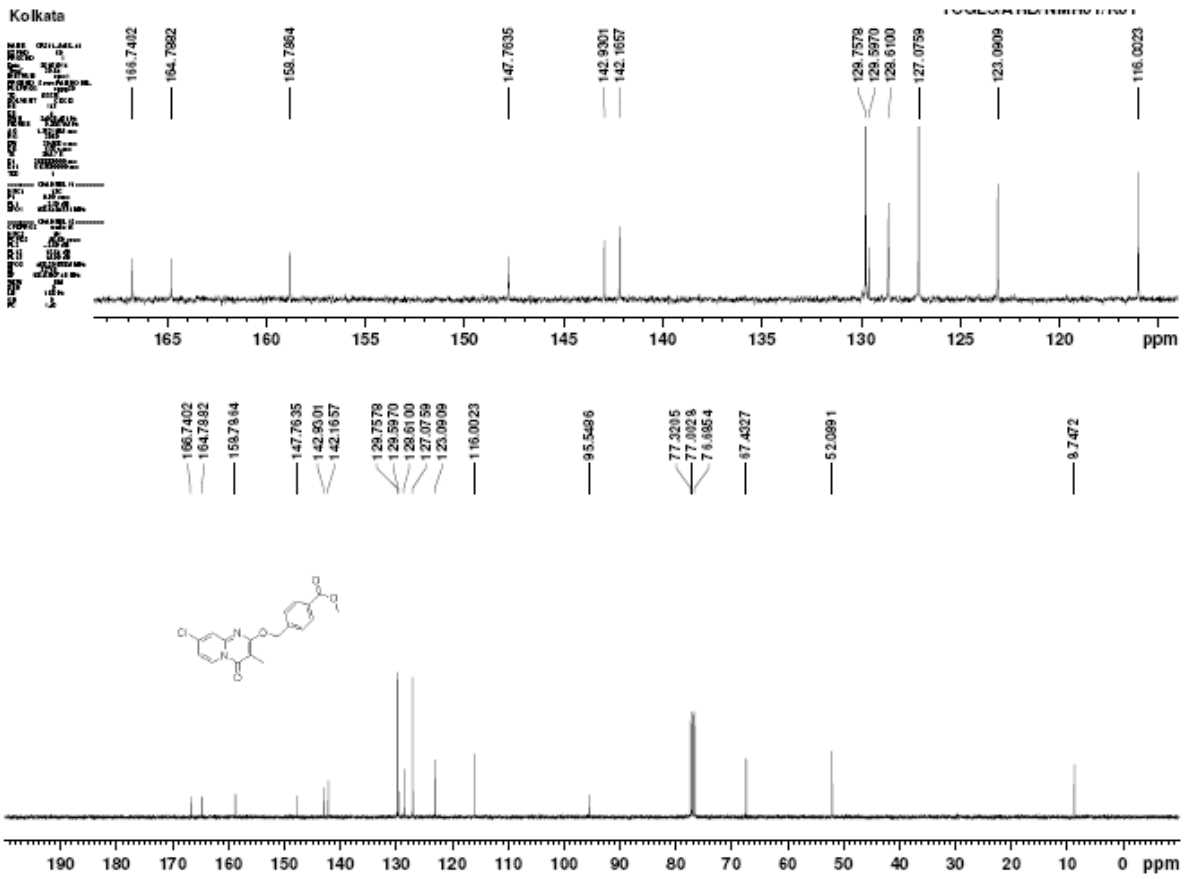

APT spectrum of compound 6b

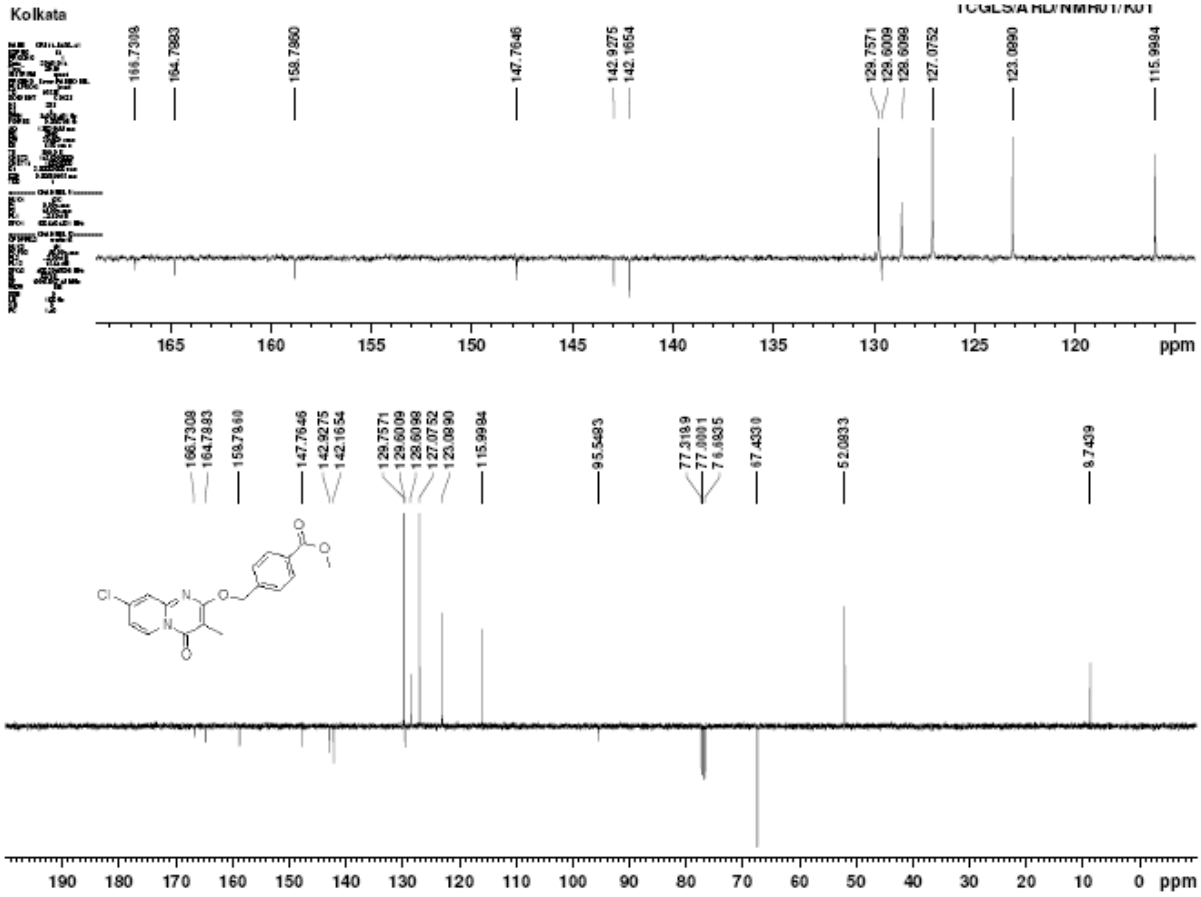

^{1}H NMR spectrum of compound 7b

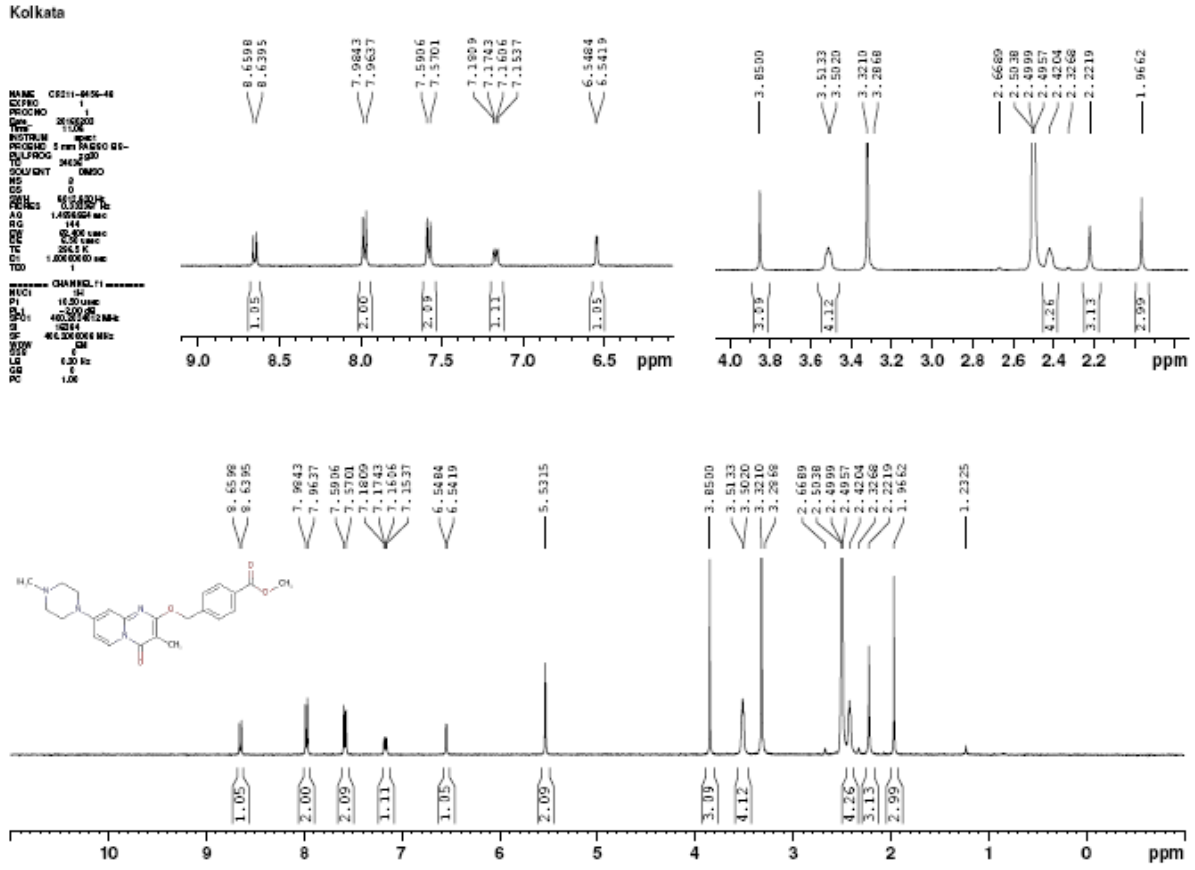

^{13}C NMR spectrum of compound 7b

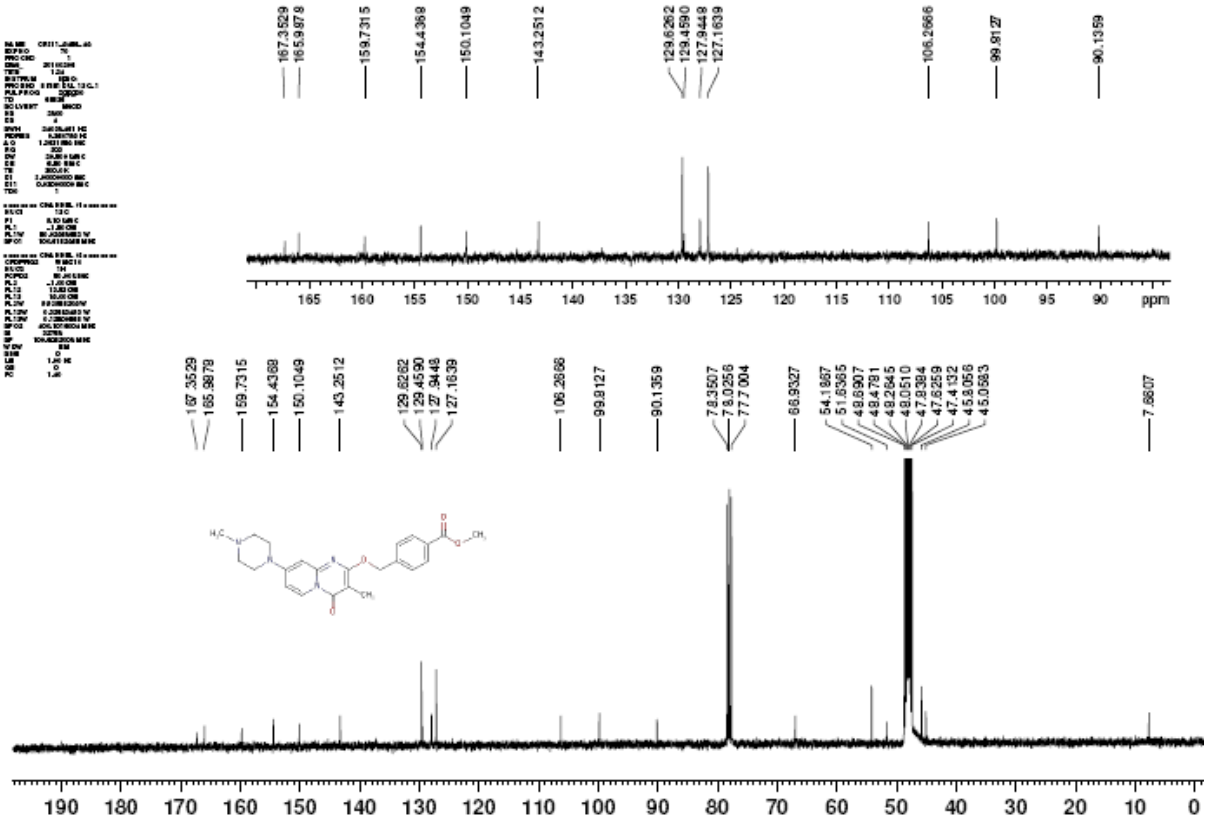

^{1}H NMR spectrum of compound 2

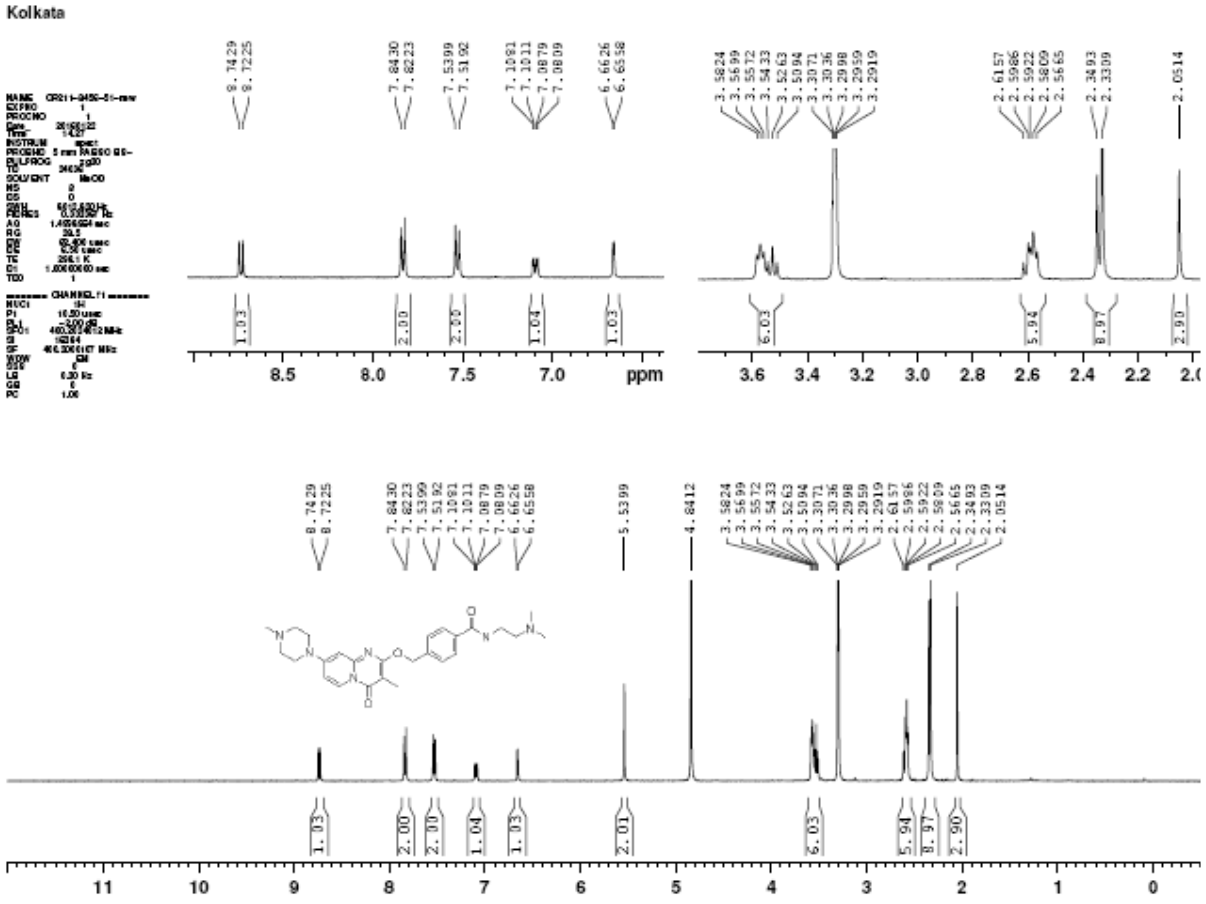

^{13}C NMR spectrum of compound 2

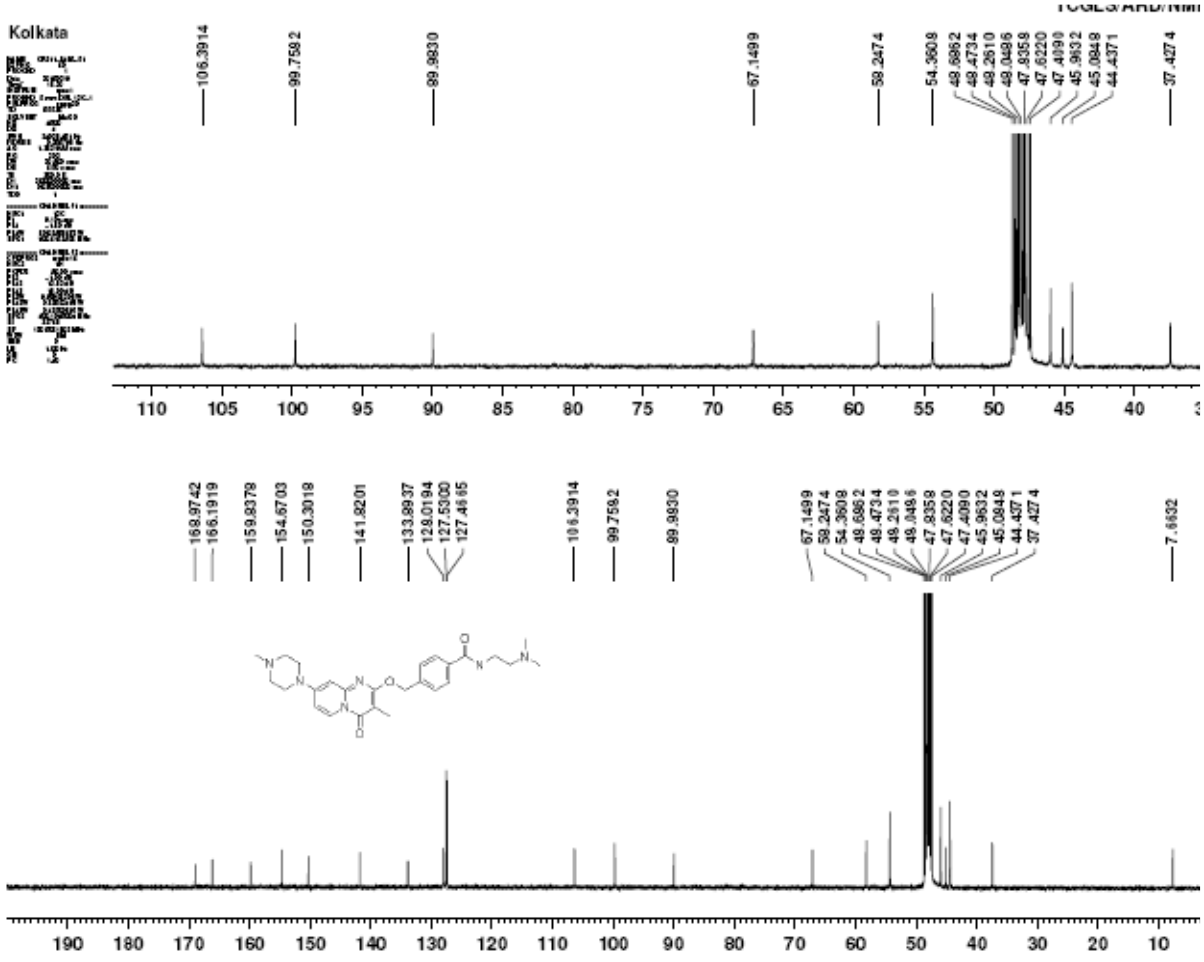

HPLC chromatogram of compound 2

```
Sample Name:CR211-8456-51-AA
Column ID:Poroshell  120 EC-C18 (4.6*100mm).2.7um; Dilu
ent: MeOH
B: ACN A : 0.05% TFA IN WATER                                                ->
Injection Date  : Fri, 29. Jan. 2016 21:36:48   Location   :    Vial 17
Sample Name     : CR211-8456-51-AA                    Inj. No.->        1
Acq Operator    : KALYAN                        Inj. Vol.  :       3 µl

Analysis Method : C:\CHEM32\1\DATA\2015\JAN-16\070116B 2016-01-07 09-1->
Last Changed    : Fri, 29. Jan. 2016, 09:54:50 pm
                  (modified after loading)

Acq. Method     : C:\CHEM32\1\DATA\2015\JAN-16\290116D 2016-01-29 19-50-
                  14\GEN_J.M
```

Ref : KB/ 29.01.16/1150

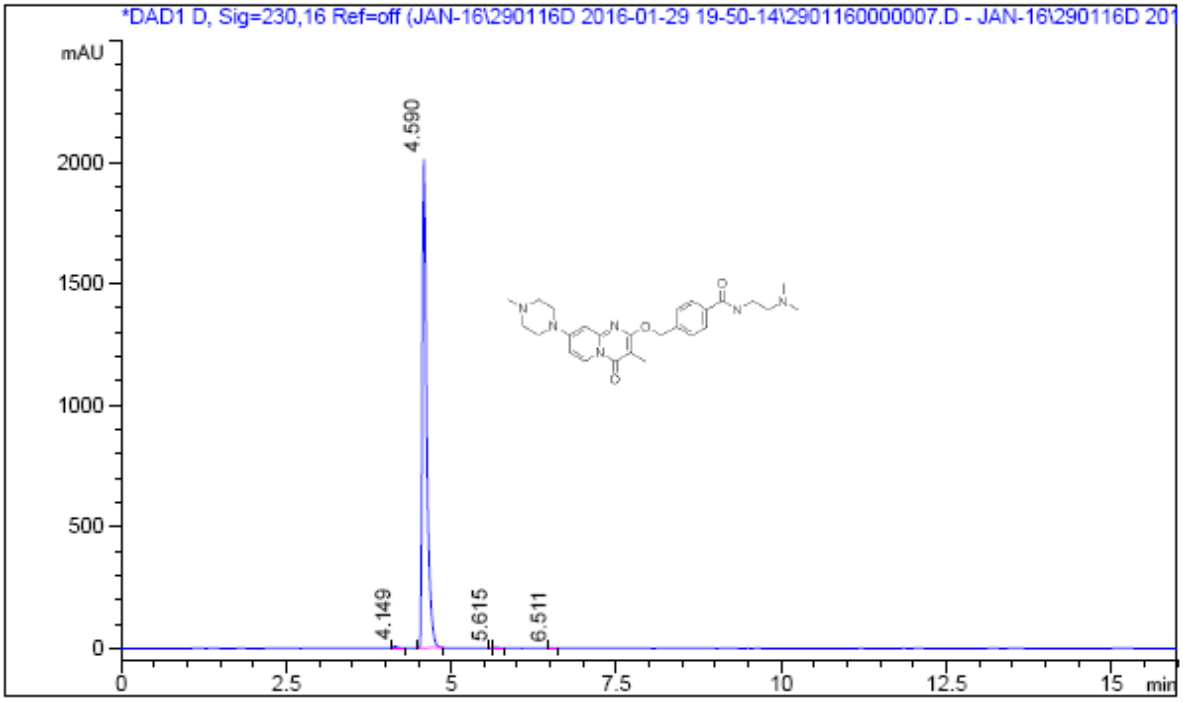


```
================================================================================

================================================================================
Signal  1 :DAD1 D, Sig=230,16 Ref=off
```

Peak #	RT [min]	Area	Area %
1	4.15	36.13	0.38
2	4.59	9356.64	99.39
3	5.62	3.47	0.04
4	5.68	14.04	0.15
5	6.51	3.84	0.04

^{1}H NMR spectrum of compound 5c

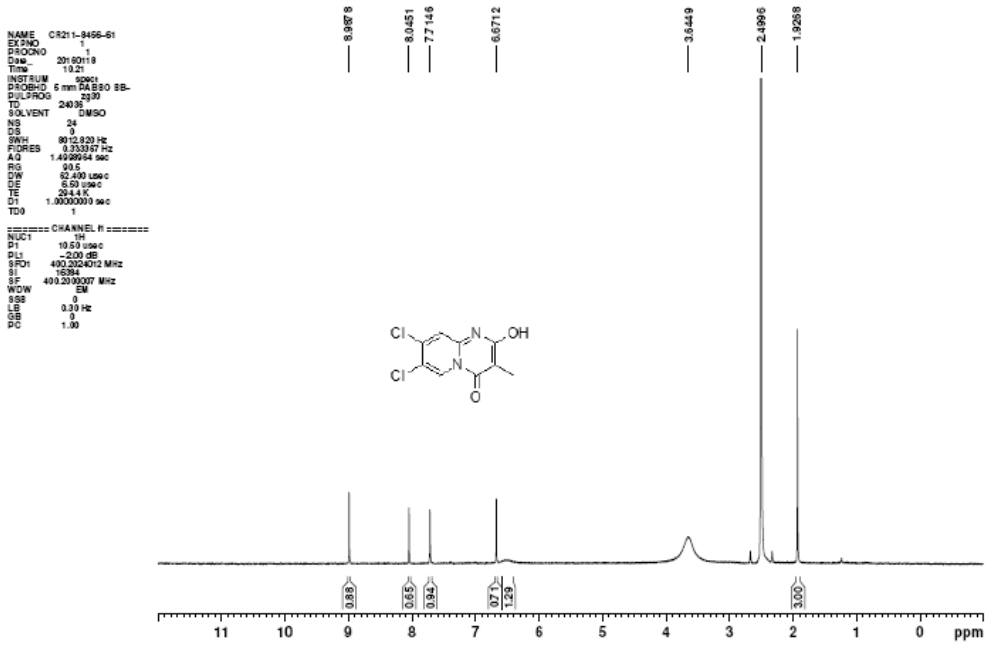

^{13}C NMR spectrum of compound 5c

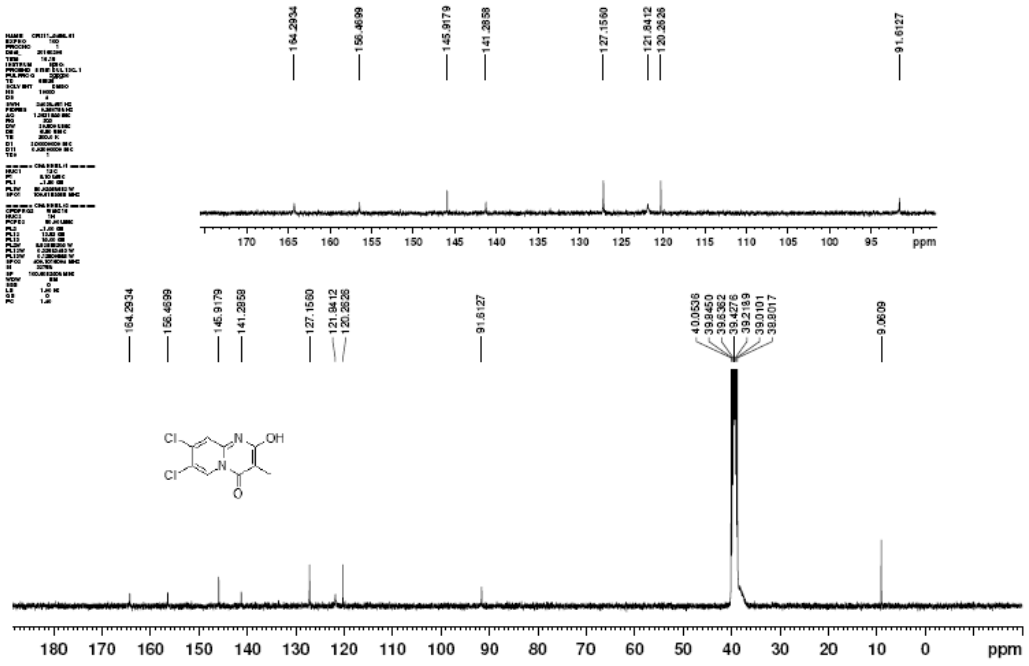

^{1}H NMR spectrum of compound 6c

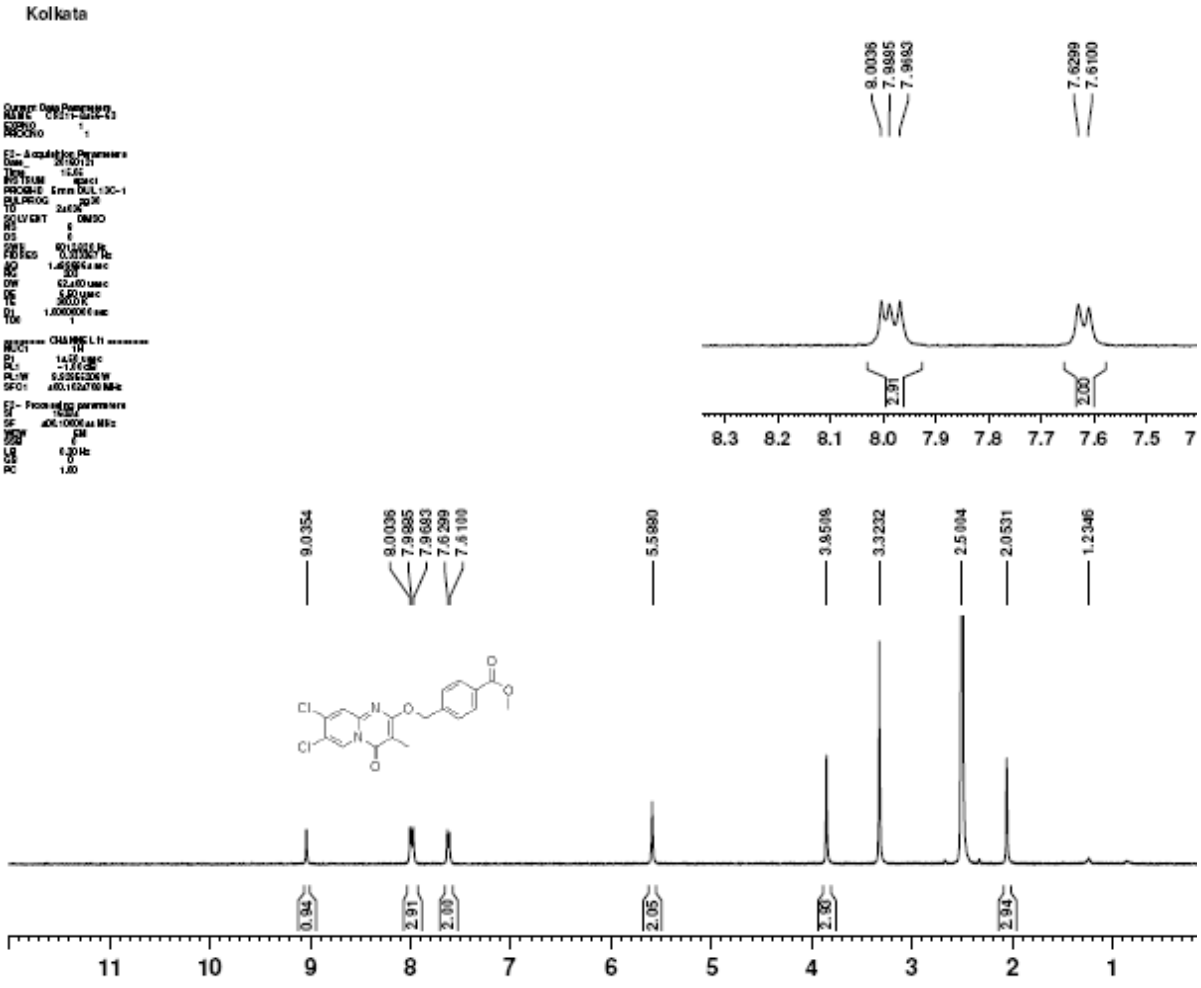

^{13}C NMR spectrum of compound 6c

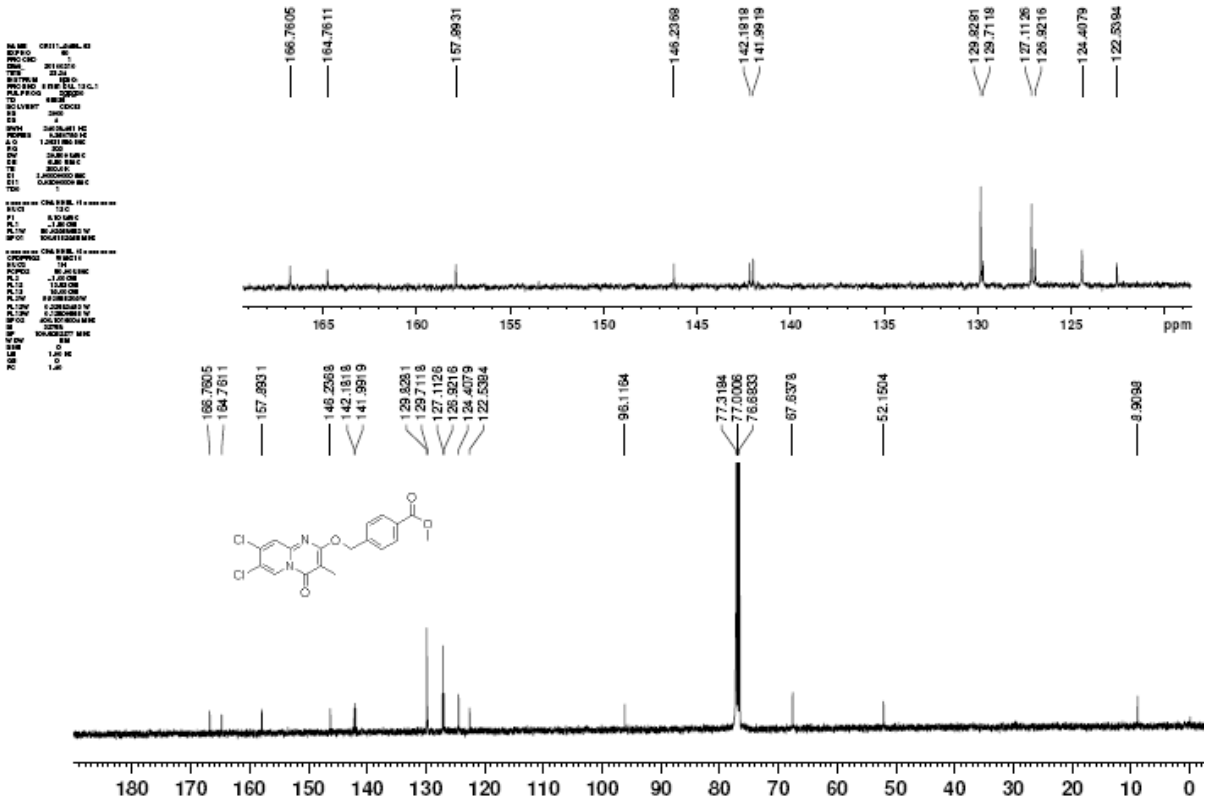

^{1}H NMR spectrum of compound 7c

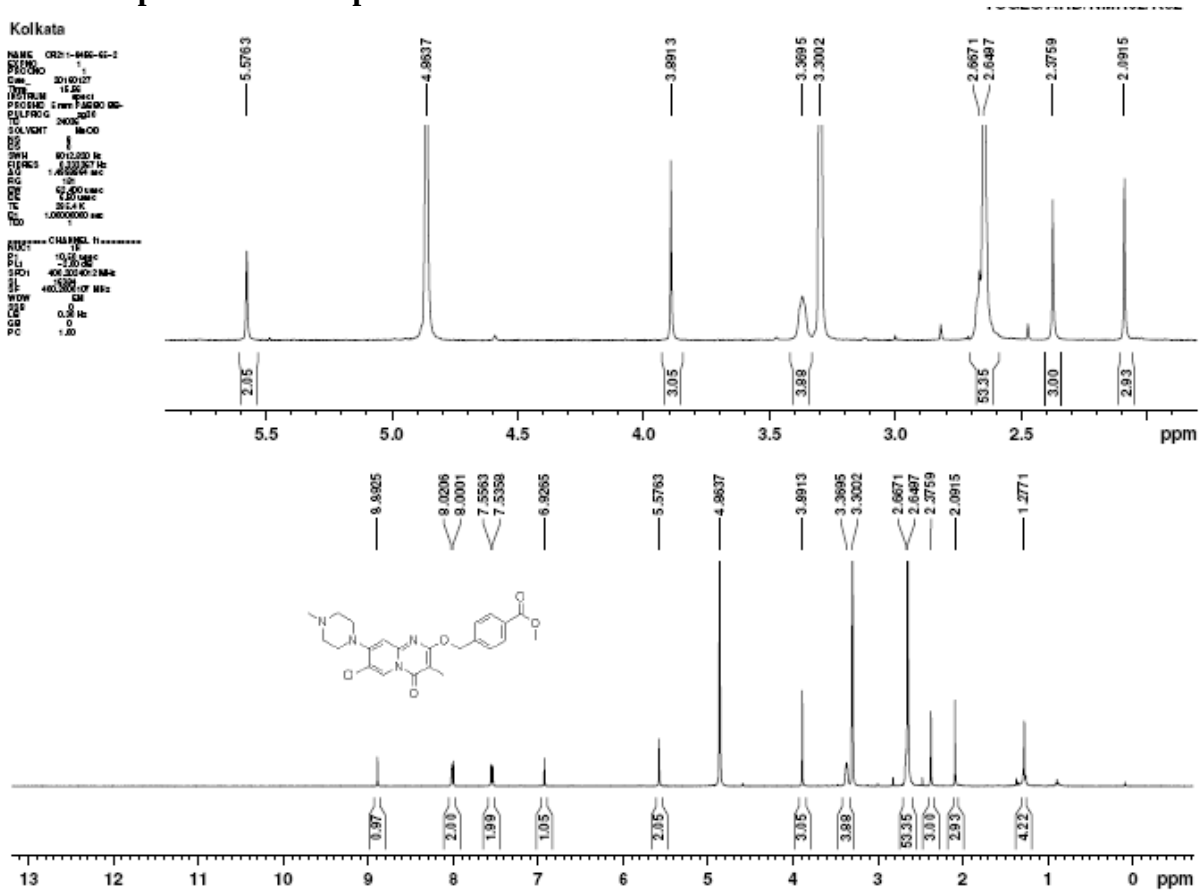

^{13}C NMR spectrum of compound 7c

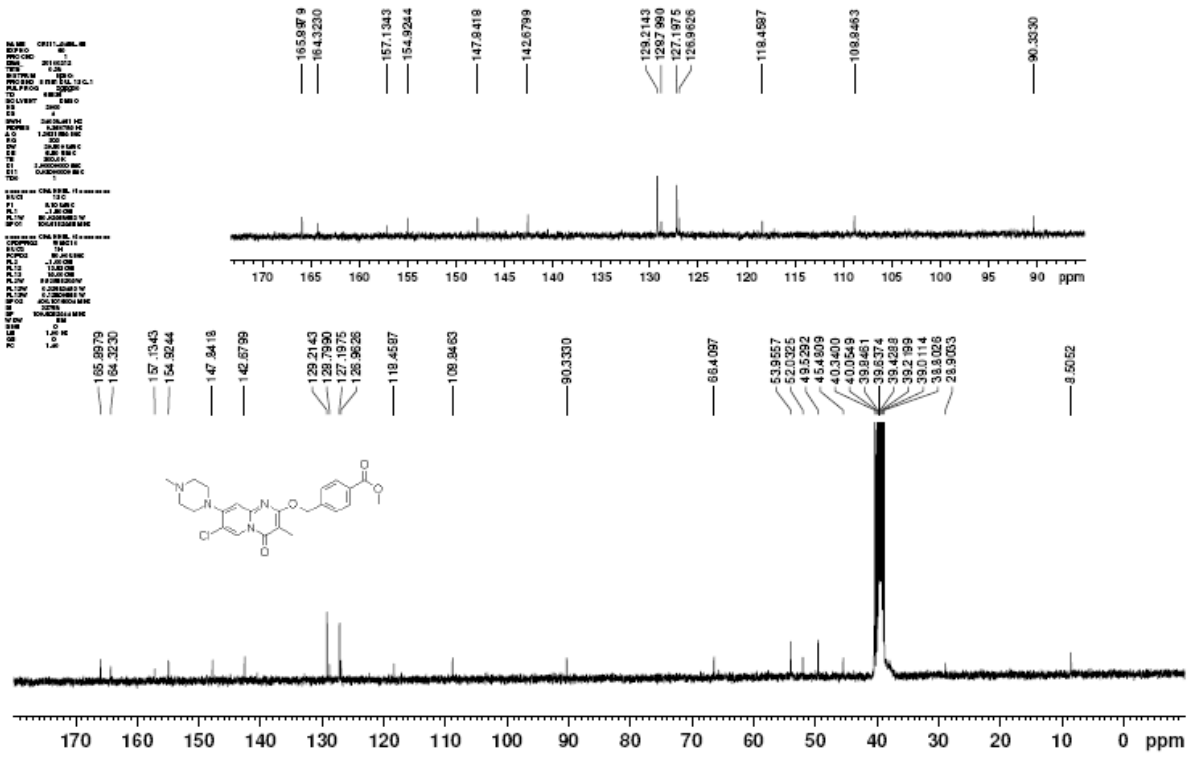

^{1}H NMR spectrum of compound 8c

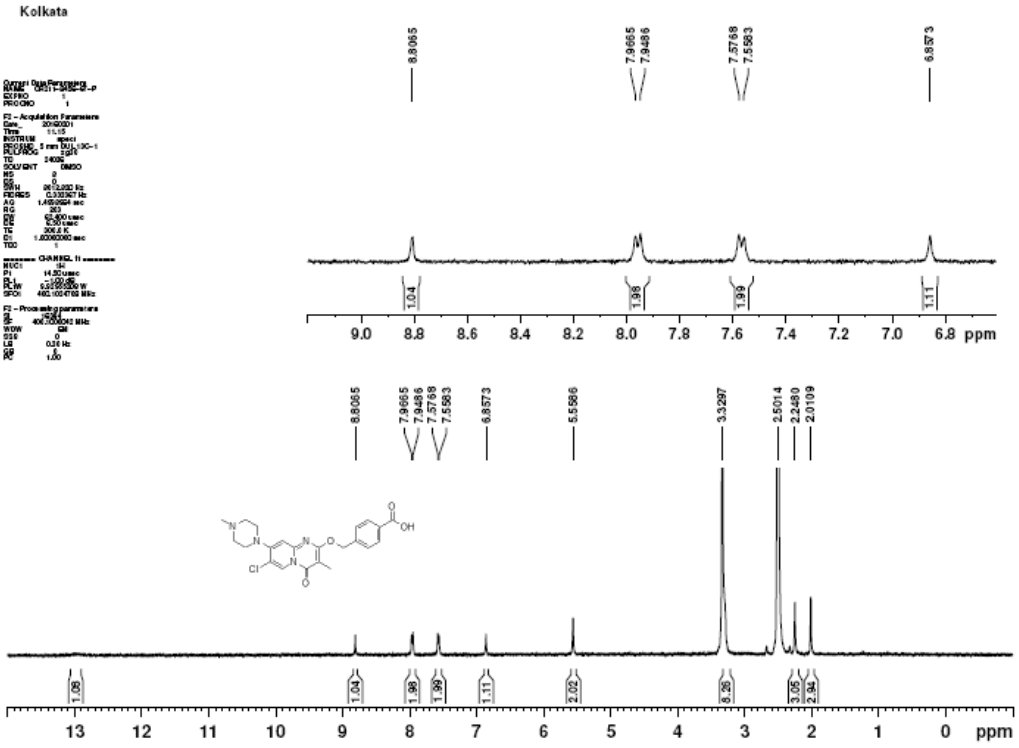

^{13}C NMR spectrum of compound 8c

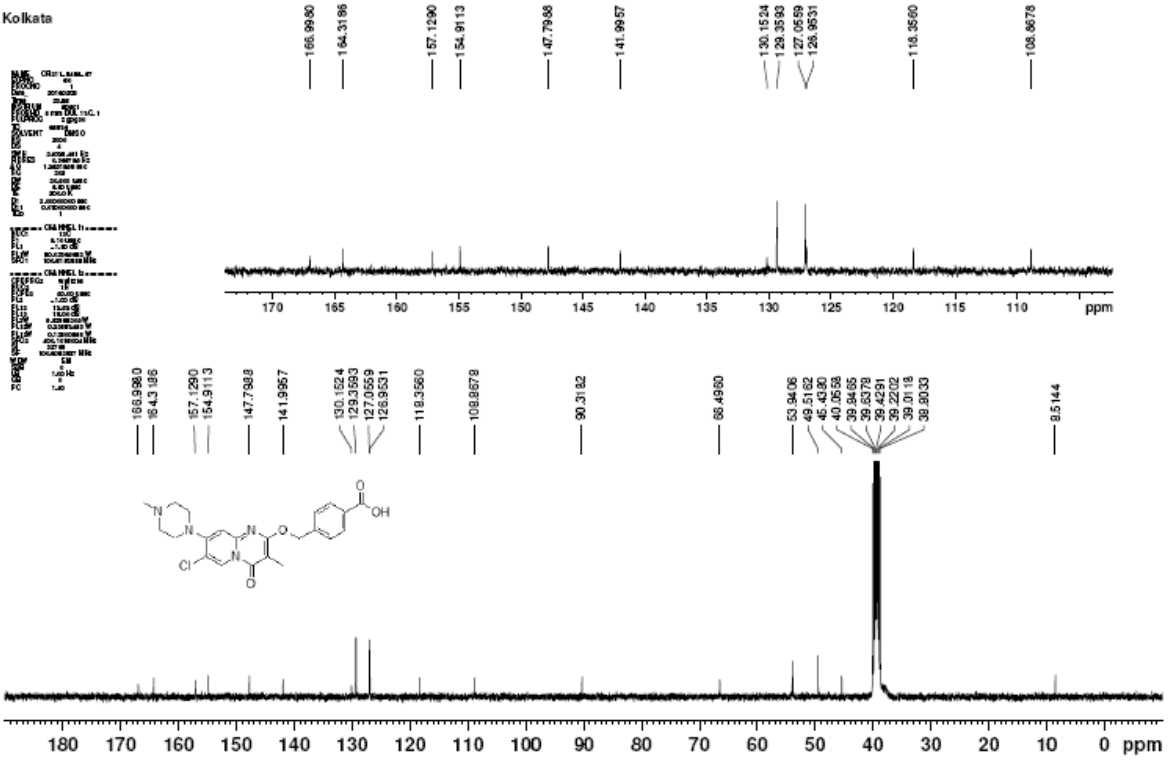

^{1}H NMR spectrum of compound 3

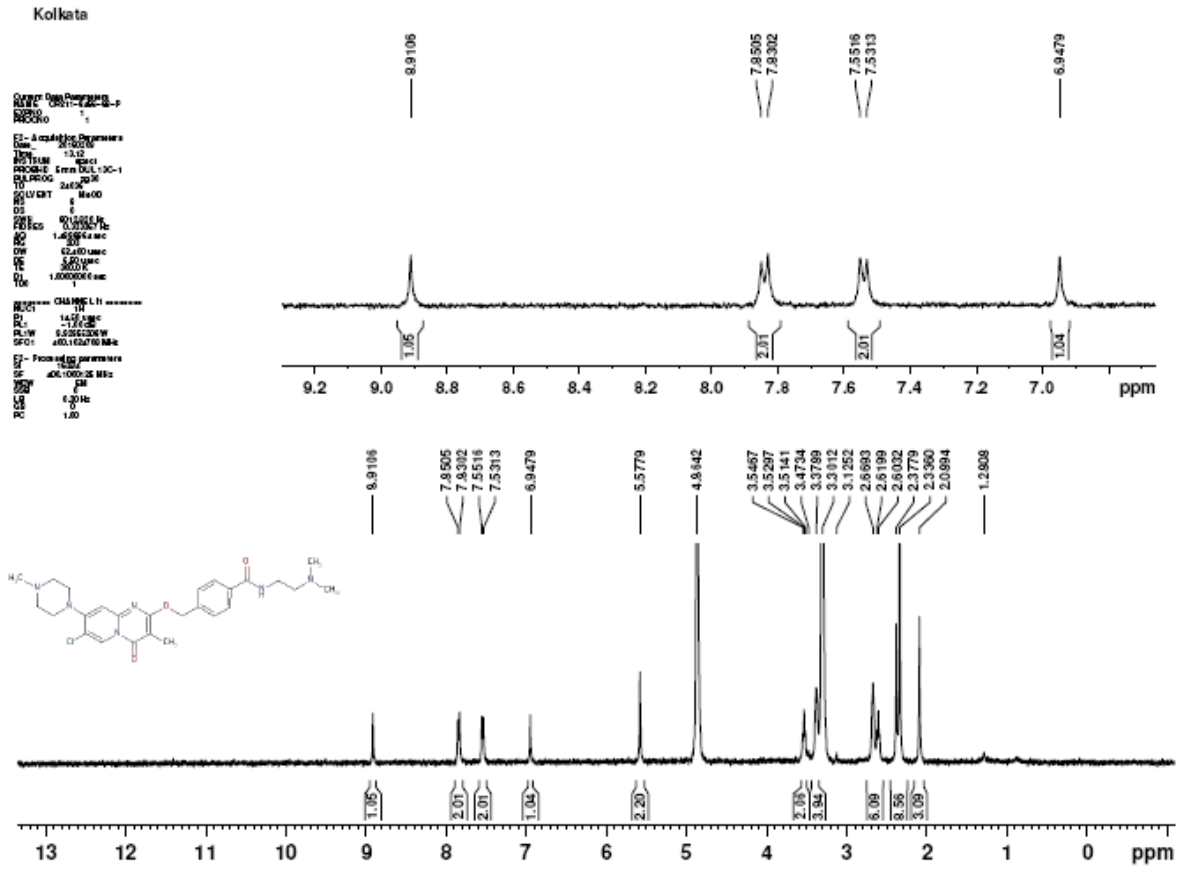

^{13}C NMR spectrum of compound 3

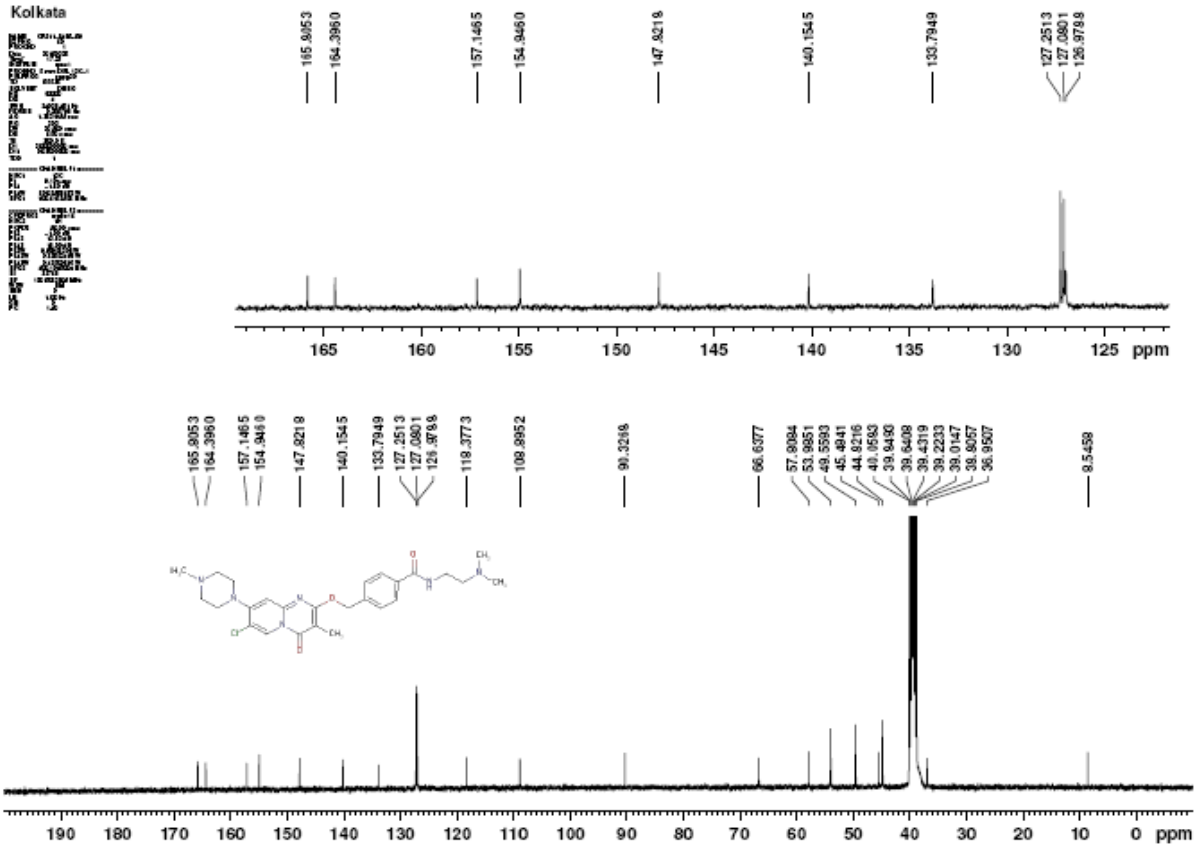

HPLC chromatogram of compound 3

```
Sample Name CR211-8456-69-P
Column ID:Poroshell  120 EC-C18 (4.6*100mm).2.7um; Dilu
ent: MeOH
B: ACN A : 0.05% TFA IN WATER                                                ->
Injection Date  : Wed, 10. Feb. 2016 11:46:25   Location   :    Vial 94
Sample Name     : CR211-8456-69-P                    Inj. No.->         1
Acq Operator    : PRIYA                          Inj. Vol.  :       4 µl

Analysis Method : C:\CHEM32\1\METHODS\GENH.M
Last Changed    : Tue, 9. Feb. 2016,  05:46:27 pm
                  (modified after loading)

Acq. Method     : C:\CHEM32\1\DATA\2015\FEB-16\100216A 2016-02-10 10-51-
                  00\GEN_J.M

                                                  Ref :PC/  10.02.16/403
```

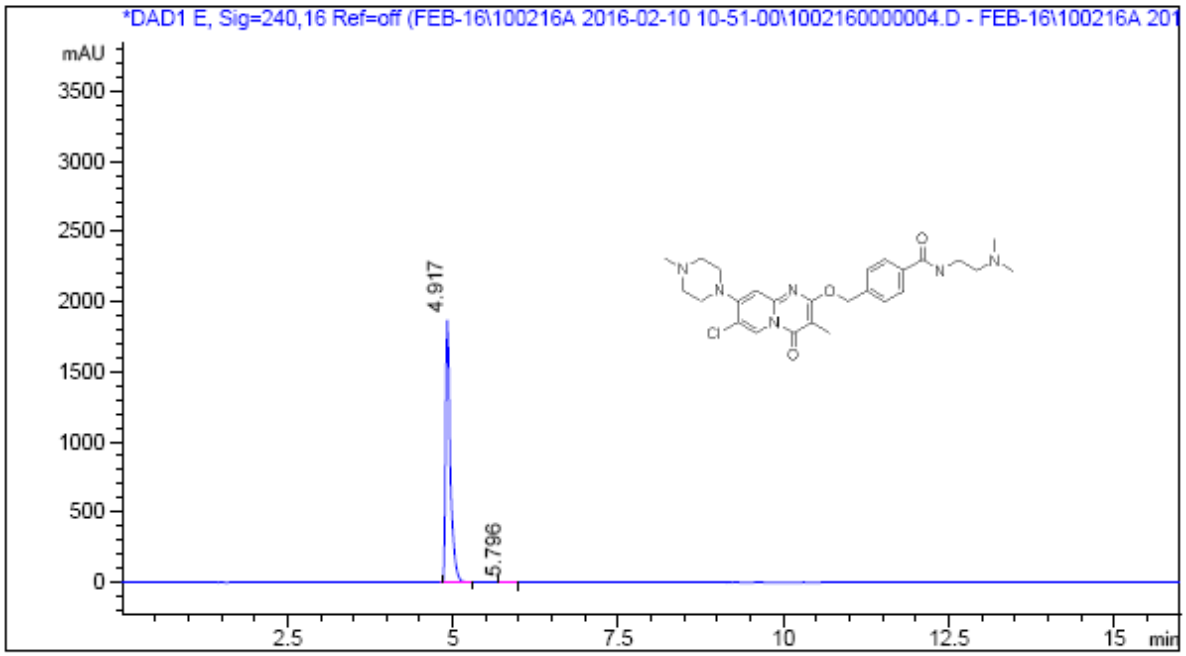


```
================================================================================

================================================================================
Signal  1 :DAD1 E, Sig=240,16 Ref=off

|Peak|   RT    |   Area    | Area % |
| #  |  [min]  |           |        |
|----|---------|-----------|--------|
|   1|     4.92|   9344.74|   99.89|
|   2|     5.80|     10.41|    0.11|
-----------------------------------
================================================================================
                        *** End of Report ***
```

References

[1] C. Plüg, B. Wallfisch, H. G. Andersen, P. V. Bernhardt, L-J. Baker, G. R. Clark, M. W. Wong, C. Wentrup, *J. Chem. Soc*. *Perkin Trans.* **2000**, *2*, 2096–2108.

[2] Frisch, M. J., Trucks, G. W., Schlegel, H. B., Scuseria, G. E., Robb, M. A., Cheeseman, J. R., Scalmani, G., Barone, V., Mennucci, B., Petersson, G. A., Nakatsuji, H., Caricato, M., Li, X., Hratchian, H. P., Izmaylov, A. F., Bloino, J., Zheng, G., Sonnenberg, J. L., Hada, M., Ehara, M., Toyota, K., Fukuda, R., Hasegawa, J., Ishida, M., Nakajima, T., Honda, Y., Kitao, O., Nakai, H., Vreven, T., Montgomery, J. A., Jr., Peralta, J. E., Ogliaro, F., Bearpark, M. J., Heyd, J., Brothers, E. N., Kudin, K. N., Staroverov, V. N., Kobayashi, R., Normand, J., Raghavachari, K., Rendell, A. P., Burant, J. C., Iyengar, S. S., Tomasi, J., Cossi, M., Rega, N., Millam, N. J., Klene, M., Knox, J. E., Cross, J. B., Bakken, V., Adamo, C., Jaramillo, J., Gomperts, R., Stratmann, R. E., Yazyev, O., Austin, A. J., Cammi, R., Pomelli, C., Ochterski, J. W., Martin, R. L., Morokuma, K., Zakrzewski, V. G., Voth, G. A., Salvador, P., Dannenberg, J. J., Dapprich, S., Daniels, A. D., Farkas, Ö., Foresman, J. B., Ortiz, J. V., Cioslowski, J., Fox, D. J., Gaussian09, Revision D.01, Gaussian, Inc.: Wallingford, CT, **2013.**

[3] J. Dai, M. Carver, L. H. Hurley, D. Yang, *J. Am. Chem. Soc*. **2011**, *133*, 17673–17680.

[4] A. T. Phan, V. Kuryavyi, S. Burge, S. Neidle, D. J. Patel, *J. Am. Chem. Soc.* **2007**, *129*, 4386–4392.

[5] D. A. Case, T. A. Darden, T. E. Cheatham, C. L. Simmerling, J. Wang, R. E. Duke, R. Luo, R. C. Walker, W. Zhang, K. M. Merz, B. Roberts, B. Wang, S. Hayik, A. Roitberg, G. Seabra, I. Kolossváry, K. F. Wong, F. Paesani, J. Vanicek, J. Liu, X. Wu, S. R. Brozell, T. Steinbrecher, H. Gohlke, Q. Cai, X. Ye, J. Wang, M. J. Hsieh, G. Cui, D. R. Roe, D. H. Mathews, M. G. Seetin, C. Sagui, V. Babin, S. Gusarov, A. Kovalenko, P. A. Kollman, *AMBER 14*, **2014**.

[6] J. Wang, R. M. Wolf, J. W. Caldwell, P. A. Kollman, D. A. Case, *J. Comput. Chem.* **2004**, *25*, 1157–1174.

[7] P.A. Kollman, I. Massova, C. Reyes, B. Kuhn, S. Huo, L. Chong, M. Lee, T. Lee, Y. Duan, W. Wang, O. Donini, P. Cieplak, J. Srinivasan, D. A. Case, T. E. Cheatham, *Acc. Chem. Res.* **2000**, *33*, 889–897.

[8] D. R. Roe, T. E. Cheatham, *J. Chem. Theory Comput.* **2013**, *9*, 3084–3095.

[9] E. F. Pettersen, T. D. Goddard, C. C. Huang, G. S. Couch, D. M. Greenblatt, E. C. Meng and T. E. Ferrin, *J. Comput. Chem.*, **2004**, *25*, 1605–1612.